

Electronic and vibrational properties of TiSe_2 in the charge-density wave phase from first principles

Raffaello Bianco, Matteo Calandra and Francesco Mauri

CNRS, UMR 7590, F-75005, Paris, France and

Sorbonne Universités, UPMC Univ Paris 06, IMPMC - Institut de Minéralogie, de Physique des Matériaux, et de Cosmochimie, 4 place Jussieu, F-75005, Paris, France

(Dated: March 11, 2015)

We study the charge-density wave phase in TiSe_2 by using first principle calculations. We show that, regardless of the local functional used and as long as the cell parameters are in agreement with the experiment, density-functional calculations are able to reproduce not only the structural instability of TiSe_2 , but also the effective distortion observed in the experiments. We study the electronic structure evolution of the system under the charge-density wave deformation. In particular, we show that the energy bands for the distorted superstructure, unfolded into the original Brillouin zone, are in reasonable agreement with angle-resolved photoemission spectroscopy (ARPES) data taken at low temperature. On the contrary, the energy bands for the undistorted structure are not in good agreement with ARPES at high temperature. Motivated by these results, we investigate the effect of the correlation on the electrons of the localized Ti- d orbitals by using the LDA+ U method. We show that within this approximation the electronic bands for both the undistorted and distorted structure are in very good agreement with ARPES. On the other hand, the U eliminates the phonon instability of the system. Some possible explanations for this counter intuitive result are proposed. Particularly, the possibility of taking into account the dependence of the parameter U from the atomic positions is suggested.

I. INTRODUCTION

The group IVb transition metal diselenide 1T- TiSe_2 (space group $P\bar{3}m1$) is a layered compound which has received considerable attention because of its interesting physical properties. In particular, below a critical temperature $T_{\text{CDW}} \simeq 200$ K it undergoes a commensurate charge density wave (CDW) transition, with the formation of a $2 \times 2 \times 2$ superlattice structure (space group $P\bar{3}c1$) accompanied by the softening of a zone boundary phonon and changes in the transport properties^{1–3}. In spite of many experimental and theoretical studies, the driving force of this structural phase transition remains controversial. Several mechanisms have been proposed for the origin of the instability in TiSe_2 and they can be roughly classified into two main groups depending on the driving role played either by the electrons or by the lattice. In fact, a charge density wave occurs always simultaneously with a periodic lattice distortions, so with both a modification of the electron and phonon spectra, but it is unclear if what is observed is primarily an instability of the electronic system or of the lattice^{4,5}. To the first case belongs the excitonic insulator model^{6–8}, where the CDW is essentially view as a many-body effect originated by the poorly screened hole-electron Coulomb interaction giving rise to a condensate of excitons and a consequent distortion. In the second family we find Peierls and Jahn-Teller band-type mechanisms^{9,10}, where the instability essentially comes from the electron-phonon coupling leading the a lattice distortion which lowers the total energy of the system. The CDW phase competes with superconductivity since TiSe_2 is not superconducting at low temperature, but CDW is suppressed and superconductivity stabilized either by Cu intercalation¹¹ or pressure¹². For

this reason, a deep and definitive understanding of the CDW occurrence would be interesting both for conceptual reasons and technological applications.

In this paper we present the specific role of the electron-phonon coupling in the appearance of the CDW ordering. As already shown in Ref. 13, thorough density functional theory (DFT) calculations it is possible to observe a structural instability at the L and M points of the Brillouin zone (BZ) consistent with a $2 \times 2 \times 2$ (L) and $2 \times 2 \times 1$ (M) real space superstructure. Here we want to provide a deeper analysis of this instability in order to find the exact distortion predicted and compare it with the experimental findings.

The paper is organized as follows: in Sec. II we summarize the method and the parameters used. Then, in Sec. III, we present the ab-initio structural analysis of the TiSe_2 instability and CDW phase. Afterwards, in Sec. IV we analyze the electronic structure of the distorted phase. Particularly, we unfold the bands of the distorted phase into the undistorted BZ in order to compare the theoretical results with the data from an ARPES experiment. In Sec. V B we show the results of the LDA+ U calculation. Finally, conclusions are presented in Sec. VI.

II. COMPUTATIONAL DETAILS

All calculations were performed within the framework of DFT using the QUANTUM ESPRESSO package¹⁴ which uses a plane-wave basis set to describe the valence-electron wave function and charge density. For the exchange-correlation functional we used both the Perdew-Zunger local density approximation (LDA)¹⁵ and the Perdew-Burke-Ernzerhof conjugate gradient approx-

TABLE I. Experimental and theoretical geometrical parameters of the system in the undistorted phase (*cf.* Fig.1): hexagonal lattice constant a , distance c between the layers, distance h between the Se and the Ti planes in a layer and horizontal projection R of distance between Se and Ti in an octahedron. The subscripts ‘Exp’ and ‘Th’ refer to the experimental and theoretical cell, respectively. Notice that for the undistorted phase R is fixed by the unit cell geometry (it must be equal to $a\sqrt{3}/3$ in order to obtain a null force along the planar direction) whereas this is not true anymore in the distorted phase (*cf.* Tab. VI).

	a (Å)	c (Å)	h (Å)	R (Å)
Exp	3.540	6.007	1.532	2.044
LDA _{Exp}	3.540	6.007	1.499	2.044
GGA _{Exp}	3.540	6.007	1.534	2.044
GGA _{Exp} ^{VdW}	3.540	6.007	1.532	2.044
LDA _{Th}	3.434	5.792	1.535	1.982
GGA _{Th}	3.536	6.719	1.548	2.041
GGA _{Th} ^{VdW}	3.510	6.165	1.553	2.026

imation (GGA)¹⁶. In the second case, as adjacent layers in TiSe₂ are coupled by Van der Waals forces, we also considered a correction to the functional¹⁷ which is aimed at describing more accurately this kind of interaction (GGA^{VdW}). In these cases the phonons have been calculated using density functional perturbation theory (DFPT) in the linear response¹⁸.

We used a cutoff of 85 Ry and 850 Ry (1 Ry \approx 13.6 eV) for the wave functions and the charge density, respectively; the BZ integration has been performed with a Monkhorst-Pack grid¹⁹ of $24 \times 24 \times 12$ \mathbf{k} and a Hermite-Gaussian smearing of 0.01 Ry. The self-consistent solution of the Kohn-Sham equations was obtained when the total energy changed by less than 10^{-10} Ry. We studied the system with internal theoretical coordinates (*i.e.* zero theoretical forces) and with both experimental and theoretical cell (*i.e.* zero theoretical pressure). The theoretical parameters have been obtained by relaxing the structure starting from the experimental parameters²⁰ until the forces on the atoms were less than 10^{-3} Ry a_0^{-1} ($a_0 \approx 0.529177$ Å is the Bohr radius) and the pressure less than 0.5 Kbar. The values of the geometrical parameters obtained for different local functionals are reported in Tab. VI. In particular, as it can be seen, the distance between the layers is underestimated in LDA and overestimated in GGA whereas, as expected, the best agreement between theory and experiment is obtained by using the GGA^{VdW} functional.

In order to take into account the strong correlation effects due to the localized d orbitals of Ti, we also considered the LDA+ U method in the simplified form described in Ref. 21,22. Since we consider one strong-correlated orbital and no spin, this adds a single additional parameter U .

We essentially performed two kind of analysis. On one hand we calculated the variation of the phonon frequencies in L and M with the value of U for the experimental

cell and theoretical internal coordinates obtained by relaxing the atomic positions for each value of U . In this case the phonon frequencies have been obtained by using the finite difference method in Ref. 23 for a $2 \times 2 \times 2$ cell with a $1/66 \simeq 0.015$ Å displacement of the atoms. A mesh grid of $24 \times 24 \times 12$ \mathbf{k} for the super-cell Brillouin zone and a Hermite-Gaussian smearing of $0.125 \cdot 10^{-2}$ Ry have been used for the related self-consistent calculations of the forces.

On the other hand we calculated, by linear response, a first-principle estimate of U for the LDA_{Exp} case in the undistorted phase, through the difference between the screened and bare second derivative of the total energy with respect to the occupation of the Ti- d orbital²¹. For an input value U_{in} , used to define the starting system, the linear-response calculation returns a different output value $U_{\text{out}} \neq U_{\text{in}}$ but, in order to be consistent and replace the LDA interaction term with the corresponding Hubbard correction, the ideal case in which $U_{\text{in}} = U_{\text{out}} \equiv U$ should be considered. In fact, even if it is a common practice to simply compute the ab-initio value of U in one step with $U_{\text{in}} = 0$, this consideration can be relevant, especially if the LDA and LDA+ U systems are qualitative different²⁴. In our case, in particular, the effect of U is to open a gap between the bands with the result of obtaining, for $U \simeq 4$, a metal-insulator transition (see Sec. VB). For this reason we determined U with a self-consistent procedure starting from the unperturbed system ($U_{\text{in}} = 0$) and using, step by step, the obtained U_{out} as U_{in} for the subsequent calculation. For each step we obtained the result first by performing the linear response calculation on a $2 \times 2 \times 2$ cell and then extrapolating the outcome to a $6 \times 6 \times 6$ cell (see Ref. 21 for details). With this procedure we converged in a few steps to the value $U \simeq 3.902$ eV. Since we decided to work with a fixed configuration, for all the steps we always kept fixed the internal coordinates equal to the ones obtained by relaxing the atomic positions with $U = 0$; moreover, in order to achieve a precision of 10^{-3} eV for the converged value of U , we set the energy convergence threshold for self-consistency equal to 10^{-14} Ry.

III. STRUCTURAL ANALYSIS OF THE CDW

In the BZ of TiSe₂ the three L points – L_1 , L_2 , L_3 – and the three M points – M_1 , M_2 , M_3 – are equivalent thanks to the three-fold rotation symmetry of the system (see Fig. 2). The vectors \mathbf{q}_{L_i} and \mathbf{q}_{M_i} from Γ to L_i and M_i , respectively, have reduced components (*cf.* Fig. 2):

$$\begin{aligned}
 \mathbf{q}_{M_1} &= \left(\frac{1}{2}, 0, 0\right) & \mathbf{q}_{L_1} &= \left(\frac{1}{2}, 0, \frac{1}{2}\right) \\
 \mathbf{q}_{M_2} &= \left(0, -\frac{1}{2}, 0\right) & \mathbf{q}_{L_2} &= \left(0, -\frac{1}{2}, \frac{1}{2}\right) \\
 \mathbf{q}_{M_3} &= \left(-\frac{1}{2}, \frac{1}{2}, 0\right) & \mathbf{q}_{L_3} &= \left(-\frac{1}{2}, \frac{1}{2}, \frac{1}{2}\right)
 \end{aligned} \tag{1}$$

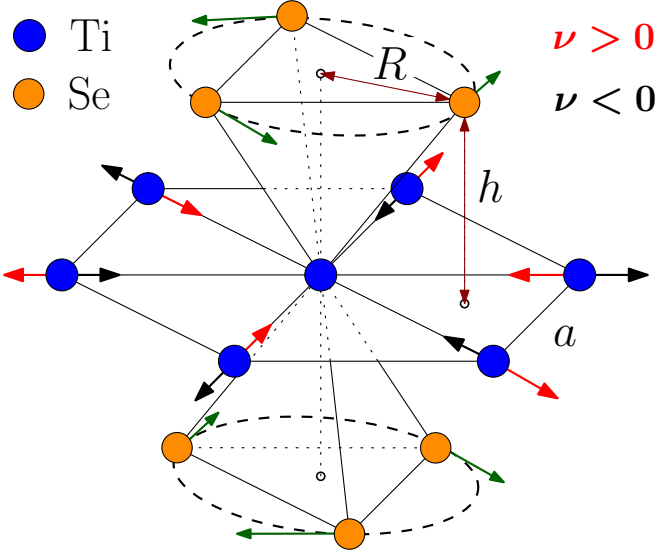


FIG. 1. (color online) Octahedral structure of TiSe_2 in a layer. The Se atoms in the upper and lower plane are on circles of radius R at distance h from the Ti atoms plane. The value of the hexagonal lattice parameter a , the distance c between two layers (not shown) and h completely define the system (the value of R is fixed by the geometry in the undistorted phase). The rotational displacement of the Se atoms in a triple- \mathbf{q} mode and the attraction (repulsion) exerted over the Ti atoms by two close Se's for $\nu > 0$ ($\nu < 0$) is also shown (see the main text for the definition of ν).

In L_i and M_i the small group is C_{2h} and the decomposition in irreducible representations is:

$$2A_u \oplus 2A_g \oplus 4B_u \oplus B_g \quad (2)$$

By using the Density Functional Perturbation Theory (DFPT) we computed the phonon frequencies at M and L . We found that in all the cases the lowest phonon mode has symmetry A_u with frequency always imaginary except in the LDA_{Th} case. The values for the phonon frequencies in the $\text{GGA}_{\text{Th}}^{\text{vdW}}$ case are shown in table Tab.II and the frequencies of the lowest mode for all the cases are reported in table Tab.III. When a phonon frequency ω is imaginary we conventionally indicate it with the negative value $-|\omega|$.

A. Ab-initio analysis of the structural instability

The imaginary phonon frequencies in M and L correspond to a structural instability consistent with a $2 \times 2 \times 1$ (M) or a $2 \times 2 \times 2$ (L) real-space superstructure. In order to study the $2 \times 2 \times 2$ distortions which lower the energy we consider the corresponding supercell of the undistorted crystal (which has 24 atoms) and the 72 dimensional space \mathcal{V} whose general element $\mathbf{d} \equiv d_{i\alpha}$ is the displacement of the i -th atom of the supercell along the cartesian coordinate α .

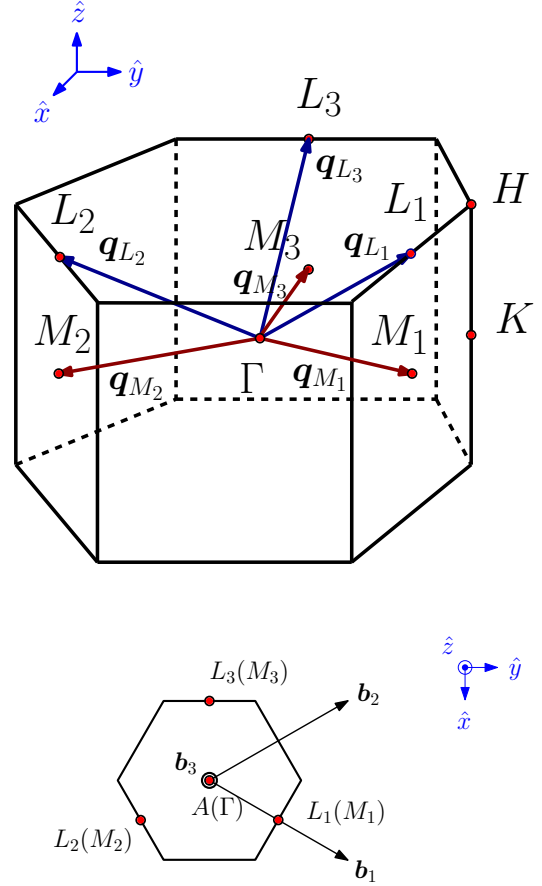


FIG. 2. Brillouin zone of TiSe_2 . The right hand figure is the BZ as seen from above. The \mathbf{b}_i are the reciprocal lattice basis vectors.

TABLE II. Phonon frequencies with relative mode symmetries at L and M in the the $\text{GGA}_{\text{Th}}^{\text{vdW}}$ case.

	ω_L (meV)	ω_M (meV)
A_u	-10.00	-9.33
B_u	12.18	12.69
A_u	14.27	14.62
B_g	17.37	17.25
B_u	17.95	17.57
A_g	20.33	20.44
A_g	23.67	23.48
B_u	24.78	24.93
B_u	37.00	37.84

TABLE III. Phonon frequencies of the lowest mode (A_u) at L and M for the cases analyzed.

	ω_L (meV)	ω_M (meV)
LDA_{Exp}	-10.38	-9.17
GGA_{Exp}	-9.83	-8.28
$\text{GGA}_{\text{Exp}}^{\text{vdW}}$	-9.61	-8.03
LDA_{Th}	+4.32	+7.13
GGA_{Th}	-13.14	-13.18
$\text{GGA}_{\text{Th}}^{\text{vdW}}$	-10.01	-9.34

For the $2 \times 2 \times 2$ superstructure the eight points Γ , A , L_i and M_i of BZ all refold to the Γ point. Thus, the space \mathcal{V} is equal to the orthogonal sum of the corresponding nine dimensional subspaces \mathcal{V}_Γ , \mathcal{V}_A , \mathcal{V}_{L_i} , \mathcal{V}_{M_i} :

$$\mathcal{V} = \mathcal{V}_\Gamma \oplus \mathcal{V}_A \oplus \mathcal{V}_L \oplus \mathcal{V}_M \quad (3)$$

$$\mathcal{V}_L \equiv \bigoplus_{i=1}^3 \mathcal{V}_{L_i} \quad \mathcal{V}_M \equiv \bigoplus_{i=1}^3 \mathcal{V}_{M_i} \quad (4)$$

whose vectors describe distortions with a definite modulation character with respect to the original $1 \times 1 \times 1$ unit cell of the undistorted phase. In particular \mathcal{V}_{L_i} and \mathcal{V}_{M_i} are made of plane-wave lattice distortions with wave vector \mathbf{q}_{L_i} and \mathbf{q}_{M_i} , respectively, that is distortions having the atomic displacement of the k -th atom in the l -th unit cell given by:

$$\mathbf{u}_{lk} = \epsilon_k \cos(\mathbf{q} \cdot \mathbf{R}_l) \quad \mathbf{q} \in \{\mathbf{q}_{L_i}, \mathbf{q}_{M_i}\} \quad (5)$$

where \mathbf{R}_l is the l -th lattice vector and ϵ_k gives the amplitude of the displacement for the k -th atom in the unit cell of the origin.

If $E(\mathbf{d})$ is the energy of the system per supercell as a function of the $2 \times 2 \times 2$ distortion, in the harmonic approximation it is:

$$E(\mathbf{d}) \simeq E(0) + \frac{1}{2} \sum_{i\alpha j\beta} \left. \frac{\partial^2 E}{\partial d_{i\alpha} \partial d_{j\beta}} \right|_{\mathbf{d}=0} d_{i\alpha} d_{j\beta} \quad (6)$$

$$\equiv E(0) + \frac{1}{2} \sum_{i\alpha j\beta} C_{i\alpha, j\beta} d_{i\alpha} d_{j\beta} \quad (7)$$

and by grouping the two indices $(i\alpha) \equiv I$ we obtain a real-symmetric 72×72 matrix C_{IJ} which has $N = 72$ couples of real eigenvalues and eigenvectors $(\lambda, \mathbf{d}^{(\lambda)})$, so that for the distortion $\mathbf{d}^{(\lambda)}$ the system has the variation of energy:

$$dE = \frac{\lambda}{2} \|\mathbf{d}^{(\lambda)}\|^2 \quad (8)$$

where $\|\mathbf{d}^{(\lambda)}\|$ is the euclidean norm of $\mathbf{d}^{(\lambda)}$. A negative eigenvalue corresponds to a displacement which lowers the energy of the system.

By using the DFPT we calculated C_{IJ} and subsequently we diagonalized it. Because of the symmetry, we obtained the same spectrum for the three spaces \mathcal{V}_{L_i} and the three spaces \mathcal{V}_{M_i} with the corresponding displacements related by threefold rotations. Consistently with the phonon analysis we found, for each of these space, two eigenspaces with symmetry A_u , one of them with negative eigenvalue. Since we are interested in the instabilities of the system we focus on this kind of distortions.

B. The A_u distortions

The displacements A_u , for a point L_i or M_i , are transversal to the direction of propagation \mathbf{q} , planar (i.e. with zero component outside the xy -plane) and opposite for selenium atoms Se_1 and Se_2 on two adjacent wave-fronts. We indicate with $-\nu$ the ratio between the displacements of the titanium atoms on a wave-front and the selenium atoms Se_1 on an adjacent wave-front:

$$A_u : \begin{cases} \epsilon_k \perp \mathbf{q} \\ \epsilon_k^z = 0 \\ \epsilon_{\text{Se}_2} = -\epsilon_{\text{Se}_1} \\ \epsilon_{\text{Ti}} = -\nu \epsilon_{\text{Se}_1} \end{cases} \quad (9)$$

Thus, the sign of ν indicates if the displacement of two adjacent Ti and Se front waves are in phase ($\nu < 0$) or out of phase ($\nu > 0$) (see Fig. 3).

These modes form a two dimensional vector space $2A_u$ made of displacements along a fixed line, where the only two free parameters left are the values of the shifts. We indicate with δTi the shift of the Ti atoms on a displacement wave-front along a given direction and with δSe the displacement of the Se atoms on an adjacent wave-front along the opposite direction (see Fig. 3). It is $\nu = \delta\text{Ti}/\delta\text{Se}$. By using the two parameters δTi , δSe the space $2A_u$ can be represented as in Fig. 4. By symmetry, two displacements with opposite values for both δTi and δSe are equivalent whereas by changing the relative phase between the shifts of the Se and the Ti atoms we obtain two different configurations. In fact, a significant parameter is the ratio ν which identifies a one dimensional subspace $A_u(\nu)$ of $2A_u$. Therefore, a general $\mathbf{d} \in 2A_u$ is uniquely identified either by ν and $\|\mathbf{d}\|$ or, for example, by ν and δTi (δSe).

Each of the two orthogonal one-dimensional eigenspaces of symmetry A_u found by diagonalizing C_{IJ} is characterized by a specific value of the ratio, one positive and the other negative. In fact, it can be shown that two generic one-dimensional subspaces $A_u(\nu_1)$ and $A_u(\nu_2)$, corresponding to different values of the ratio $\nu = \nu_1$ and $\nu = \nu_2$, are orthogonal if and only if $\nu_1 \nu_2 = -2$. We found that, in all the studied cases and in both the points M and L , the A_u with the smallest eigenvalue λ corresponds always to the positive ratio $\nu > 0$, that is to the out of phase distortion. The values found for the smallest λ and the corresponding ν in the point L (λ_L, ν_L) and M (λ_M, ν_M), for all the cases, are reported in Tab. IV. From now on we analyze only the cases where the system displays instability, so we do not consider LDA_{Th} anymore.

The value ν_L (ν_M) defines (up to a sign) three orthogonal unit vectors $\hat{\mathbf{d}}_{L_i}$ ($\hat{\mathbf{d}}_{M_i}$) corresponding to degenerate displacements of type A_u which generate a three dimensional space \mathcal{V}_L^- (\mathcal{V}_M^-). By considering displacement vectors \mathbf{d} in this space with an increasing modulus $\|\mathbf{d}\|$ but fixed direction, we can study the energy variation of the system along a pattern. We observe that the energy, after

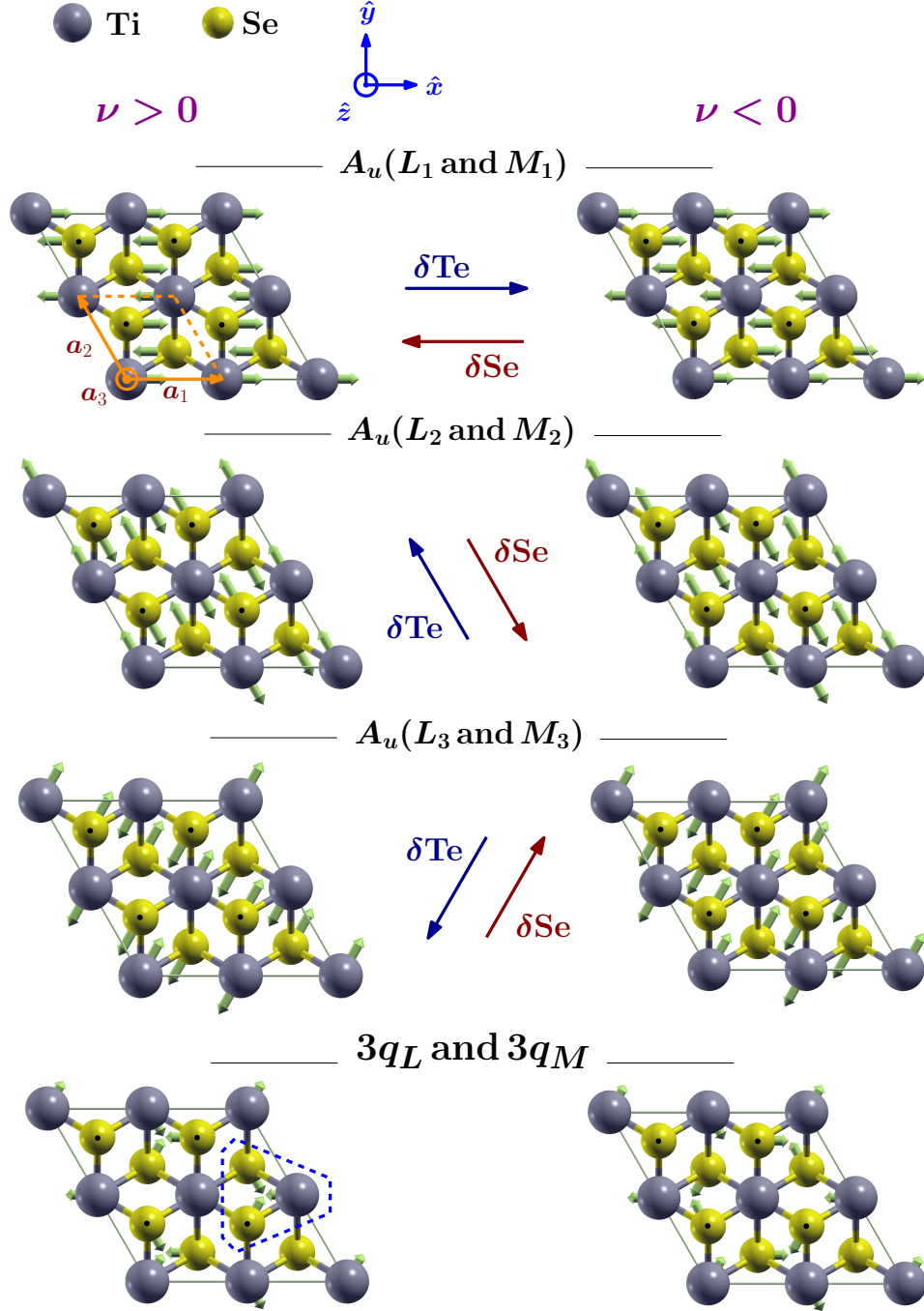


FIG. 3. (color online) Schematic representation of the atomic displacements in the $2 \times 2 \times 2$ cell of a single layer viewed from above for the three A_u modes in the points L_i and M_i and the triple modes $3q_L$ and $3q_M$. Both the not equivalent cases for $\nu > 0$ (left-hand figures) and $\nu < 0$ (right-hand figures) are shown, ν being the ratio between δTi and δSe . The Se atoms with a dot are on the upper plane with respect to the Ti atoms plane. In the first picture it is also drawn the direct lattice basis \mathbf{a}_i and the $1 \times 1 \times 1$ unit cell. The two central arrows indicate the positive directions used to measure the shifts δTi and δSe . In the $3q$ mode with $\nu > 0$ a three atom cluster is highlighted with a dotted line. Notice that the triple- q modes shown are not equal to the sum of the A_u single- q modes represented as, otherwise, the displacements should be larger (the displacements of the atoms in a triple mode are two times larger than the displacements of the component single modes).

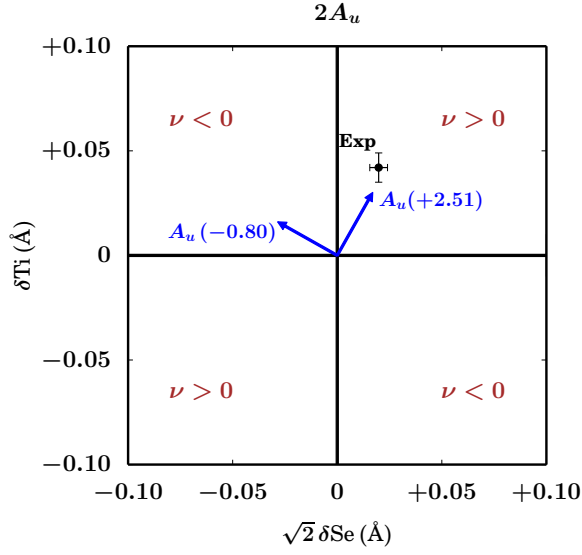


FIG. 4. (color online) Diagram representing the distortion space $2A_u$ in L and M as a function of the displacements (δSe , δTi). The factor $\sqrt{2}$ on the horizontal axis comes from the two Se atoms in the unit cell and it is necessary in order to convert the orthogonality condition in $2A_u$ into the euclidean orthogonality on the diagram. A line on this plot represents a one dimensional subspace $A_u(\nu)$ with a specific ratio $\nu = \delta\text{Ti}/\delta\text{Se}$. As an example, the two orthogonal vectors corresponding to the A_u distortion modes of the $\text{GGA}_{\text{Th}}^{\text{vdW}}$ case are drawn. The point corresponding to the CDW distortion experimentally observed¹ is also drawn.

TABLE IV. Values of the eigenvalue λ and the ratio $\nu = \delta\text{Ti}/\delta\text{Se}$ for the A_u distortions in L and M corresponding to the smallest eigenvalue. Last row: value of the ratio measured for the CDW distortion¹.

	λ_M	ν_M	λ_L	ν_L
LDA_{Exp}	-1.07	2.89	-1.37	2.93
GGA_{Exp}	-0.89	2.60	-1.26	2.53
$\text{GGA}_{\text{Exp}}^{\text{vdW}}$	-0.84	2.64	-1.20	2.56
LDA_{Th}	+0.69	2.34	+0.25	2.42
GGA_{Th}	-2.26	2.46	-2.25	2.43
$\text{GGA}_{\text{Th}}^{\text{vdW}}$	-1.14	2.51	-1.31	2.46
$\nu_{\text{CDW}}^{\text{Exp}}$	—	—	—	3.42 ± 1.48

an initial parabolic decrease, starts departing from the harmonic regime, reaches a minimum and then increases (*cf.* Fig. 5). The minimum along this energy path corresponds to the configuration which gives the most stable structure obtainable with that kind of distortion. In general, different patterns in \mathcal{V}_L^- (\mathcal{V}_M^-) return different results as for finite displacements the symmetries of the lattice are not preserved.

C. The single-point and triple-point patterns

The displacement pattern of type A_u characterized by a unit vector \hat{d}_{L_i} (\hat{d}_{M_i}) is also called a *single- \mathbf{q}_L pattern* (*single- \mathbf{q}_M pattern*). In Fig. 5 we show, for the several studied cases, the energy path for the single- \mathbf{q} patterns in L and M . As we can see the distortion of type L returns always a structure more stable than the distortion of type M , except in the GGA_{Th} case where the two energy patterns approximatively coincide, meaning that the interaction between layers plays a not negligible role in the minimization of the total energy unless their distance is large enough. Moreover, as long as the cell dimensions are comparable, we find similar results irrespective of the local functional used. Instead in the GGA_{Th} case, where the volume of the unit cell is larger (see Tab. VI), the energy gain due to the distortion is higher. These considerations leads to the conclusion that the suppression of the instability in the LDA_{Th} case is ascribable to a pure volume effect, since the LDA theoretical unit cell is smaller than the experimental one (see Tab. VI).

The pattern characterized by the unit vectors \hat{d}_{3L} and \hat{d}_{3M} obtained by combining the three directions \hat{d}_{L_i} and \hat{d}_{M_i}

$$\hat{d}_{3M} \equiv \sum_{i=1}^3 \frac{1}{\sqrt{3}} \hat{d}_{M_i} \quad \hat{d}_{3L} \equiv \sum_{i=1}^3 \frac{1}{\sqrt{3}} \hat{d}_{L_i} \quad (10)$$

are called a *triple- \mathbf{q}_L ($3\mathbf{q}_L$) pattern* and a *triple- \mathbf{q}_M ($3\mathbf{q}_M$) pattern*, respectively. In fact, by definition, a general triple- \mathbf{q} distortion of type L (M) is obtained by superimposing, with equal weights, three A_u distortions for the points L_i (M_i) having the same values of δTi and δSe .

In a layer, the shifts of the atoms in a $3\mathbf{q}$ distortion can be described by considering the TiSe_6 octahedral structure of the system²⁵ (see Fig. 1). We distinguish two kinds of Ti and Se atoms: in one the $\text{Ti}(\alpha)$ atoms do not move and are in the middle of an octahedron $\text{Ti}(\alpha)\text{Se}(\alpha)_6$ where the three $\text{Se}(\alpha)$ atoms above $\text{Ti}(\alpha)$ and the three $\text{Se}(\alpha)$ atoms below $\text{Ti}(\alpha)$ rotate with opposite direction. Thus, there are couples of $\text{Se}(\alpha)$'s which become closer and, depending on whether the component three modes have $\nu > 0$ or $\nu < 0$, they attract or repulse a $\text{Ti}(\beta)$ atom (in the first case, as a consequence, we observe a $\text{Ti}(\beta)$ - $\text{Se}(\alpha)$ bond shortening and the formation of three-atoms clusters $\text{Ti}(\beta)\text{Se}(\alpha)_2$ in the system). In the distortion we also have $\text{Se}(\beta)$ atoms which are not involved in any rotation (they are originally in octahedra centered around $\text{Ti}(\beta)$ atoms) but stay in their position.

For an adjacent layer, depending on whether we are considering a $3\mathbf{q}_M$ or a $3\mathbf{q}_L$ distortion, the displacement of the atoms is the same or the opposite one (*i.e.* in the $3\mathbf{q}_L$ case if in one layer the $\text{Se}(\alpha)$'s on the upper plane and lower plane show a clockwise and a counterclockwise rotation the opposite happens in an adjacent layers, respectively). Two $3\mathbf{q}$ distortions with $\nu > 0$ and $\nu < 0$, in a layer and view from above, are shown in Fig. 3.

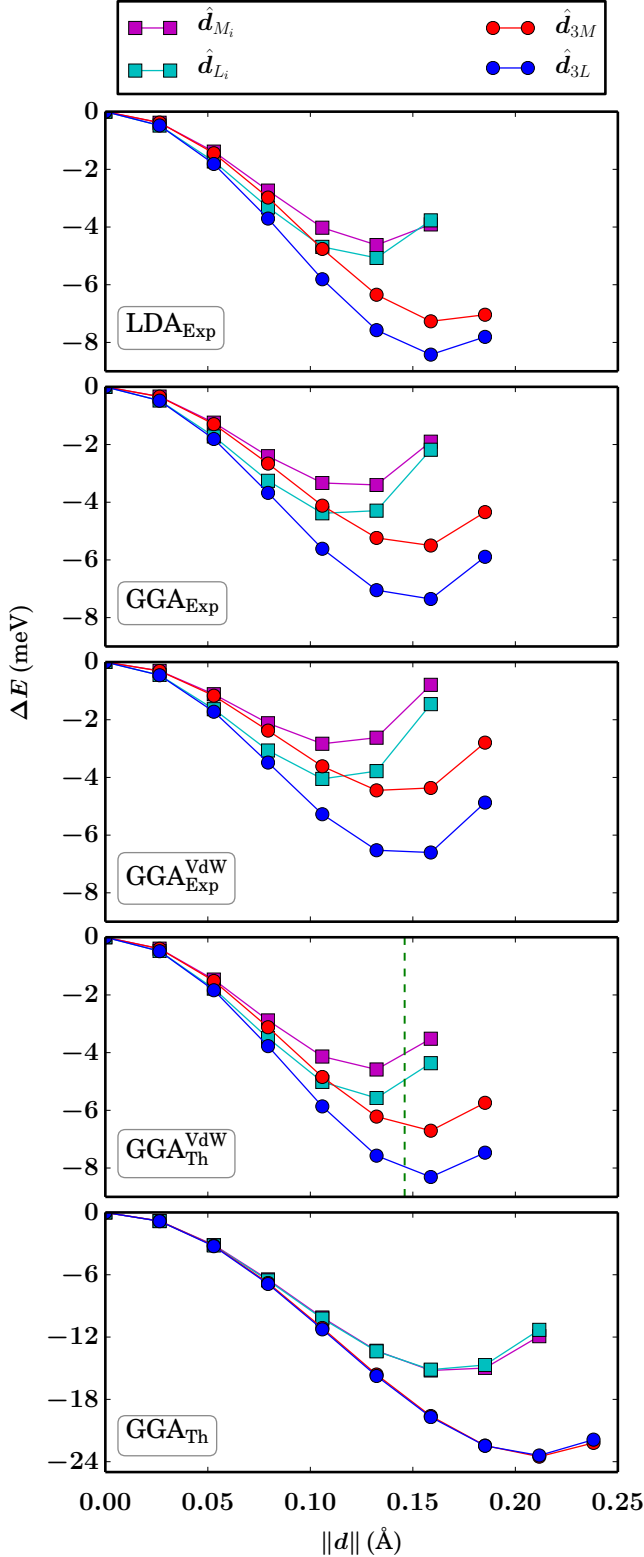


FIG. 5. (color online) Variation of the energy with respect to the undistorted phase obtained by moving the atoms according to different patterns. The unit vectors $\hat{d}_{L_i}, \hat{d}_{M_i}, \hat{d}_{3L}, \hat{d}_{3M}$ characterize a single \mathbf{q}_{L_i} and \mathbf{q}_{M_i} mode, and a triple \mathbf{q}_L and \mathbf{q}_M mode, respectively. The vertical dashed line in the $\text{GGA}_{\text{Th}}^{\text{VdW}}$ plot marks the point where the calculations of Fig. 7 have been performed.

D. The CDW distortion

In their seminal paper Di Salvo and coworkers stated that, according to neutron-diffraction measurements and symmetry considerations, the lattice distortion experimentally observed with the CDW is a $3\mathbf{q}_L$ mode with $\nu > 0$, with data taken at 77 K which best fitted with the values¹:

$$\begin{aligned}\delta\text{Ti}^{\text{Exp}} &= (0.042 \pm 0.007)\text{\AA} \\ \delta\text{Se}^{\text{Exp}} &= (0.014 \pm 0.004)\text{\AA}\end{aligned}\quad (11)$$

for the displacements of the atoms in the single L_i component modes. These values correspond, for the complete $3L$ pattern, to the displacements:

$$\begin{aligned}\delta\text{Ti}^{(3)}{}^{\text{Exp}} &= (0.085 \pm 0.014)\text{\AA} \\ \delta\text{Se}^{(3)}{}^{\text{Exp}} &= (0.028 \pm 0.007)\text{\AA}\end{aligned}\quad (12)$$

for the Ti and Se atoms which actually move (in a $3\mathbf{q}$ mode not all the atoms move). The experimental values for the displacements in a single \mathbf{q}_{L_i} component mode are also shown on the diagram in Fig. 4 and correspond to the experimental estimate for the ratio:

$$\nu^{\text{Exp}} \equiv \delta\text{Ti}^{\text{Exp}} / \delta\text{Se}^{\text{Exp}} = 3.42 \pm 1.48 \quad (13)$$

Motivated by these experimental results we calculated the energy pattern of the $3\mathbf{q}_L$ mode in \mathcal{V}_L^- for the several studied cases. Moreover, in order to study the role played by the interaction between layers, we also calculated the energy pattern of the $3\mathbf{q}_M$ distortion in \mathcal{V}_M^- . The results are shown in Fig. 5. As we can see a triple- \mathbf{q} pattern returns always a structure more stable than the corresponding single- \mathbf{q} displacement and it is always the $3\mathbf{q}_L$ distortion which gives the lowest energy (except in the GGA_{Th} case where the modes $3\mathbf{q}_L$ and $3\mathbf{q}_M$ are almost degenerate). Moreover, as for the single- \mathbf{q} patterns, when the cell dimensions are comparable we find similar results, irrespective of the local functional used.

In Tab. V we report, for the minimum point of the $3\mathbf{q}_L$ energy pattern, the values of the energy variation (per supercell) and the shift of the atoms (for the component A_u single- \mathbf{q}_L modes) with respect to the undistorted crystal. The values of the displacements for the several cases, compared with the experimental result, are also shown in Fig. 6 (which corresponds to a portion of the diagram in Fig. 4).

The fact that a $3\mathbf{q}_L$ pattern gives a structure more stable than the single \mathbf{q}_L pattern is in agreement with the experimental findings but, in order to demonstrate that the ab-initio calculations are able to predict the experimental results, it is necessary to go further and demonstrate that the $3\mathbf{q}_L$ pattern gives the most stable structure among all the possible distortions in \mathcal{V}_L^- . Since we expected analogous results in all the cases analyzed we just considered the $\text{GGA}_{\text{Th}}^{\text{VdW}}$ one. In order to accomplish the

TABLE V. First column: largest energy gain (per supercell), with respect to the undistorted phase, for the $3\mathbf{q}_L$ triple pattern in \mathcal{V}_L^- . Second and third columns: corresponding atomic displacements, with respect to the undistorted phase, for the component single modes (A_u symmetry). Notice that for the resultant $3\mathbf{q}_L$ mode the displacement of the atoms which actually move is two times larger, *cf.* Fig. 3. First row: experimental measure of the displacement for the CDW phase with respect to the high-temperature phase¹.

	$\Delta E^{\min}(\text{meV})$	$\delta\text{Ti}(\text{\AA})$	$\delta\text{Se}(\text{\AA})$
EXP	—	0.042 ± 0.007	0.014 ± 0.004
LDA _{Exp}	-8.4	0.030	0.010
GGA _{Exp}	-7.4	0.027	0.011
GGA _{Exp} ^{VdW}	-6.8	0.026	0.010
GGA _{Th}	-23.4	0.037	0.015
GGA _{Th} ^{VdW}	-8.3	0.028	0.011

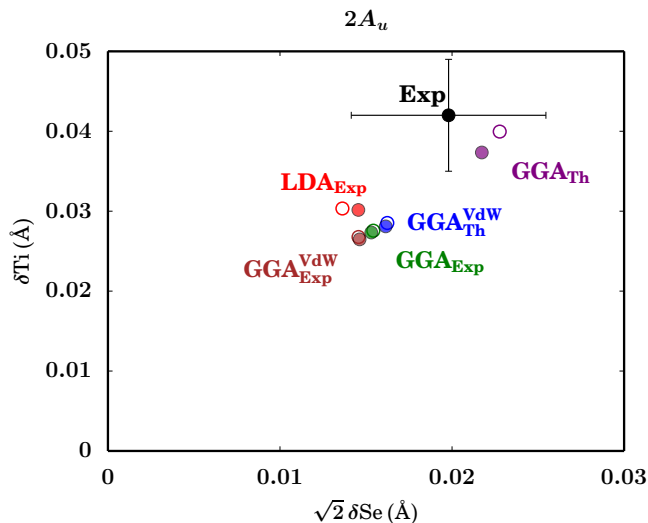


FIG. 6. (color online) Filled points: displacement of the atoms corresponding to the energy minimum along the $3L$ pattern in \mathcal{V}_L^- (single A_u component). Empty points: A_u component of the total displacement obtained by further relaxing the structure.

task, we should have considered a uniform sample of the unit sphere in \mathcal{V}_L^- and computed the energy path for an increasing modulus of the distortion along each of these directions. Instead, in order to reduce the workload, we just computed the energy of the system for distortions \mathbf{d} having a fixed modulus $\|\mathbf{d}\| = \mathcal{D}$, where $\mathcal{D} = 0.146\text{\AA}$ is a length approximately in half position between the minimum along the \mathbf{q}_{L_i} and the $3\mathbf{q}_L$ patterns (*cf.* Fig. 5). In this way we only needed to scan the energy of the system for a uniform grid on the two dimensional sphere in \mathcal{V}_L^- with radius \mathcal{D} . We used the basis $\hat{\mathbf{d}}_{L_i}$ to parametrize the space \mathcal{V}_L^- and the fact that given a general vector $\mathbf{d} = \sum_{i=1}^3 c_i \hat{\mathbf{d}}_{L_i}$ all the other vectors obtained from it by changing the sign of its components c_i give equivalent distortions. Therefore, we considered only one octant of

the sphere of radius \mathcal{D} to obtain a general scan of the surface:

$$\mathbf{d} = \sum_{i=1}^3 c_i \hat{\mathbf{d}}_{L_i} \quad \sum_{i=1}^3 |c_i|^2 = \mathcal{D} \quad c_i > 0 \quad (14)$$

An heatmap plot of the results obtained is showed in Fig. 7: our calculations confirm that on this sphere the $3\mathbf{q}_L$ pattern (which has components $c_i = \mathcal{D}/\sqrt{3}$) returns, among all the possible patterns in \mathcal{V}_L^- , the most stable structure. We conclude that, in the frame of the electron-phonon interaction, by using first-principle calculations we are able to recover the CDW structural instability experimentally observed for TiSe₂.

E. Optimization of crystal structure in the CDW phase

In order to find the equilibrium configuration for the distorted system we subsequently relaxed the structure starting from the configuration corresponding to minimum of the energy along the $3\mathbf{q}_L$ path. We relaxed the whole structure (cell and internal positions) or only the internal positions depending on whether we were considering the theoretical or the (fixed) experimental cell. This led to a further small gain in energy with respect to the undistorted phase (see Tab. VI).

As it can be seen from Tab. VII, the effect of the relaxation on the lattice parameters is quite small, with a relative variation of the order of 10^{-3} . For the internal displacements we define the vectors in \mathcal{V} , \mathbf{d}^{\min} and \mathbf{d}^{rlx} , characterizing the atomic shifts from the undistorted phase to the minimum along the $3\mathbf{q}_L$ path in \mathcal{V}_L^- and the equilibrium position reached after the relaxation, respectively (in the theoretical cell cases \mathbf{d}^{rlx} is the relative displacement with respect to the cell). A quantitative measure of the extent of the additional atomic displacements due to the relaxation is obtained by comparing the modulus and the direction of these vectors. The results are shown in Tab. VII and, as we can see, the two vectors are very similar (only slightly different in the GGA_{Th} case), meaning that the relaxation does not give an additional huge displacement of the atoms.

The displacement of the atoms due to the optimization is obviously restricted by the symmetry of the distorted phase. The total displacements \mathbf{d}^{rlx} is mainly made of a $3\mathbf{q}_L$ distortion but it also has a small component which changes the value of R shown in Fig. 1 (the value of this parameter being not fixed by the symmetry, anymore) and modifies the distances h_α and h_β between the not equivalent Se(α) and Se(β) atoms and the Ti plane. As a consequence, in the distorted structure the upper (and lower) Se atoms of a layer are not on the same plane anymore (*cf.* also Ref. 26). The values found for the atomic displacements are reported in Tab. VI and, in

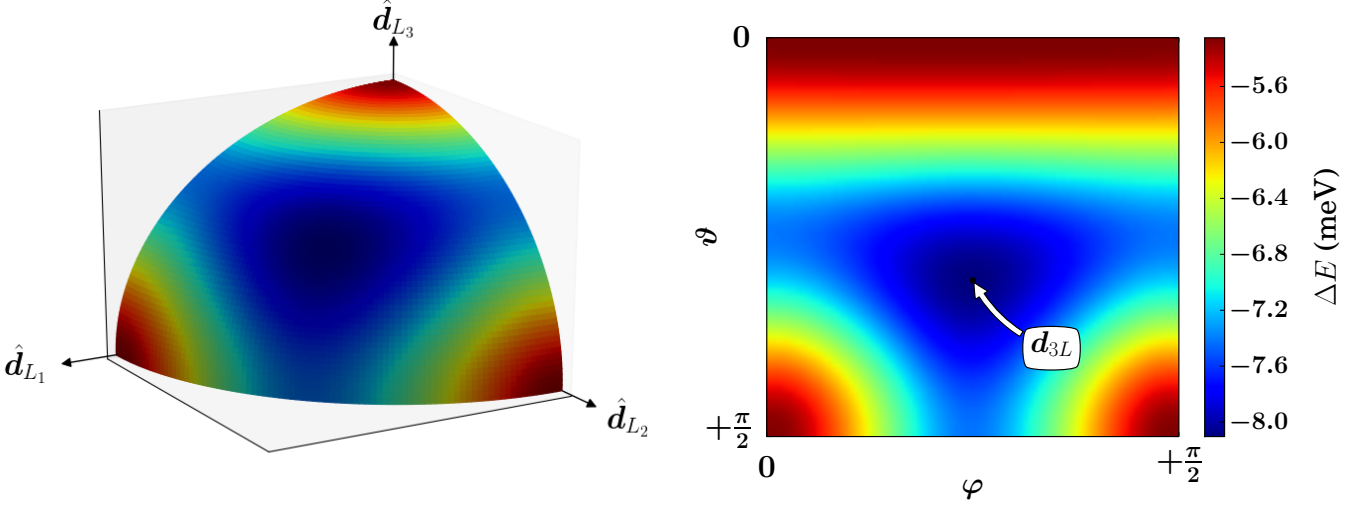


FIG. 7. (color online) GGA_{Th}^{VdW} case: heatmap plot of the energy variation with respect to the undistorted phase for distortions corresponding to vectors in \mathcal{V}_L^- having modulus $\mathcal{D} = 0.146 \text{ \AA}$. Due to the symmetry of the system the result is shown on a single octant. Left hand panel: 3D color plot on the spherical surface of radius \mathcal{D} . Right hand panel: 2D plot in spherical coordinates (ϑ, φ) associated to the basis $(\hat{\mathbf{d}}_{L_i})$. The lowest energy is obtained for the $3\mathbf{q}_L$ distortion, whose angular coordinates are $\varphi = \pi/4$, $\vartheta = \arccos(1/\sqrt{3})$.

TABLE VI. Effect of the relaxation on the minimum of the energy along the $3\mathbf{q}_L$ path in \mathcal{V}_L^- : total variation of the energy (per supercell) from the undistorted phase ΔE^{rlx} , shifts δTi and δSe for the A_u component of the atomic displacements, variation of R (see Fig. 1), and change of h for the two not equivalent atoms $\text{Se}(\alpha)$ and $\text{Se}(\beta)$. First row: experimental measure of the displacement for the CDW phase with respect to the high-temperature phase¹.

	$\Delta E^{\text{rlx}}(\text{meV})$	$\delta\text{Ti}(\text{\AA})$	$\delta\text{Se}(\text{\AA})$	$\delta R/R$	$\delta h_\alpha/h$	$\delta h_\beta/h$
EXP	—	0.042 ± 0.007	0.014 ± 0.004	—	—	—
LDA _{Exp}	-9.4	0.030	0.010	-0.0003	0.0011	-0.0001
GGA _{Exp}	-8.7	0.028	0.011	-0.0003	0.0016	0.0004
GGA _{Exp} ^{VdW}	-7.9	0.027	0.010	-0.0002	0.0014	0.0004
GGA _{Th}	-27.6	0.040	0.016	-0.0018	0.0031	-0.0038
GGA _{Th} ^{VdW}	-9.5	0.029	0.011	-0.0004	0.0010	-0.0006

TABLE VII. Effect of the relaxation on the minimum of the energy along the $3\mathbf{q}_L$ path in \mathcal{V}_L^- : variation of the cell parameters a and c (in the theoretical cell cases) and comparison of the vectors \mathbf{d}^{min} and \mathbf{d}^{rlx} representing the shifts of the internal atomic positions from the undistorted phase to, the minimum of the energy along the $3\mathbf{q}_L$ path and the final relaxed configuration, respectively.

	$\frac{\ \mathbf{d}^{\text{rlx}}\ }{\ \mathbf{d}^{\text{min}}\ }$	$\frac{\langle \mathbf{d}^{\text{rlx}} \mathbf{d}^{\text{min}} \rangle}{\ \mathbf{d}^{\text{rlx}}\ \ \mathbf{d}^{\text{min}}\ }$	$\frac{\Delta a}{a}$	$\frac{\Delta c}{c}$
LDA _{Exp}	1.0008	0.9992	—	—
GGA _{Exp}	1.0016	0.9981	—	—
GGA _{Exp} ^{VdW}	1.0022	0.9985	—	—
GGA _{Th}	1.0392	0.9918	0.0006	0.0013
GGA _{Th} ^{VdW}	1.0046	0.9990	0.0006	0.0006

particular, the updated values of δTi and δSe for the A_u component of the displacement are also shown in Fig. 6.

In conclusion, the energy gain and the A_u component of the atomic displacements obtained in all the studied cases are similar for similar unit cell and the atomic shifts are not far from the experimental measures. In particular, the ab-initio calculations based on the electron-phonon interaction predict the correct displacement pattern for the low energy distortion with the values of the atom displacements slightly underestimated (especially for the Ti). Only for the GGA_{Th} case, which however uses cell parameters quite different from the experimental ones, we have found different results with, in particular, a larger atomic displacement and a larger energy decrease for the low temperature phase with respect to the other cases.

F. Chiral Charge-Density Waves

Quite recently, on the basis of tunneling microscopy²⁷ and x-ray scattering²⁸ measurements, it has been reported the existence of a second phase transition for TiSe_2 which follows the conventional CDW transition and occurs at temperature around 7 K below the T_{CDW} . As we have seen, the conventional CDW transition is due to the superposition with equal weights of three modes describing a charge transfer process from $\text{Ti-}3d$ to $\text{Se-}4p$ orbitals and a related commensurate lattice distortion. The new type of transition is still given by the sum of these three charge transfer waves but with different relative phases, producing an helical distribution of charge along the z axis of the $2 \times 2 \times 2$ cell. As a consequence, there are two possible, energetically degenerate, distributions of charge characterizing two chiral phases related by a mirror transformation. These are the so called Chiral Charge-Density Waves (CCDW) and a driving mechanism for chiral symmetry breaking it has also been proposed.²⁹ One of the most important features of CCDW transition is the reduction of the crystal symmetry from a threefold to a twofold rotation symmetry.

In our simulations we did not see any evidence for a phase different from the conventional CDW: the lowest total energy for the system was obtained by considering the superimposition of the three modes with equal weights. Nonetheless, we find worthwhile to stress that, by using a very simple argument, it is still possible to explain the existence of different chiral domains on the surface of a TiSe_2 sample (but not the change of symmetry). As shown in Fig. 1, the CDW transition is characterized, in a cell, by a clockwise or counterclockwise rotation of the Se atoms in the upper layer (and the opposite for the Se in the bottom layer). Thus, for a cell, there are two possible degenerate but different CDW structures that cannot be superimposed solely with rotational transformations and this could naturally led to the formation, on the surface of a TiSe_2 sample, of two different chiral domains. We think that this aspect should be properly taken into account when the results of an experiment about the CCDW is interpreted. For the same reason, we believe that a simple surface experiment, like a scanning tunnel microscopy measure, could be misleading and that only a measure of the symmetry change of the crystal can prove the existence of a second phase transition different from the conventional CDW.

IV. ELECTRONIC STRUCTURE IN THE CDW PHASE

A. Undistorted energy bands

In this section we discuss the evolution of the DFT band structure under the lowest energy distortion found in \mathcal{V}_L^- . In Fig. 8 we can see the undistorted bands of TiSe_2 around the Fermi level (E_F) for an high-symmetry

path (*cf.* Ref. 30). The atomic/orbital character of the bands is also shown (*cf.* Ref. 26). In all the cases we find similar results: around the Fermi level there are only $\text{Ti-}3d$ and $\text{Se-}4p$ derived bands with a narrow $\text{Ti-}3d$ band which is almost entirely unoccupied except around the L point where it crosses the Fermi level and forms a hole pocket; moreover, two $\text{Se-}p$ and $\text{Ti-}d$ strongly hybridized bands cross the Fermi level. A qualitative difference is instead found for a narrow $\text{Se-}4p$ band whose position mostly depends on the cell dimensions (in particular on the distance between the Se and the Ti atom planes) but not on the local functional used. In fact, as we increase the value of c we observe a lowering of the band maximum in Γ (in addition to an increase of the structural instability, as we have seen in the previous section). Nevertheless, as we will see, this band does not change during the distortion.

B. Energy bands and DOS in the CDW phase

We are interested in the evolution of the band structure induced by the $2 \times 2 \times 2$ distortion. From now on we consider the cases LDA_{Exp} and $\text{GGA}_{\text{Th}}^{\text{vdW}}$. With the subscript ‘sc’, set below the labels Γ, M, K of the special points in the BZ, we refer to the corresponding points of the $2 \times 2 \times 2$ super-cell Brillouin zone (SBZ) which has the same shape of the BZ but half size.

In Fig. 9 we show the $2 \times 2 \times 2$ bands, around the Fermi level, for an high symmetry line of the SBZ for the undistorted and distorted phase, the last one corresponding to the minimum of the energy along the $3q_L$ distortion path in \mathcal{V}_L^- . On formation of the superstructure we observe a neat change near the Fermi level with similar characteristics in the two cases. In particular, around Γ_{sc} we find avoided crossings at the Fermi level and, just below it, the appearance of a (reversed) Mexican-hat structure due to the repulsion of bands having $\text{Ti-}3d$ character (see Fig. 9). The $\text{Se-}4p$ bands crossing the Fermi level around the wave vector $(1/2)\Gamma_{\text{sc}}M_{\text{sc}}$, instead, do not suffer any modification during the distortion, as anticipated. As expected, the change of the electronic dispersion around the Fermi leads to a change of the Density of States (DOS) as it is shown in Fig. 10. On forming the superlattice structure the DOS decreases by around 40% at E_F and a peak, essentially due to the $\text{Ti-}4d$ orbitals, develops at 0.15/0.2 eV below E_F . These effects have been qualitatively observed in some previous theoretical works (see Ref. 31, for example, for a tight-binding study) and are, at some level, compatible with the change of the resistivity experimentally observed in the CDW transition¹.

C. Energy bands folding and unfolding

The superlattice distortion doubles the original lattice periodicity of the system. In fact, each eigenfunction $\Psi_{\mathbf{K},j}$ of the distorted system has the pseudo-momentum

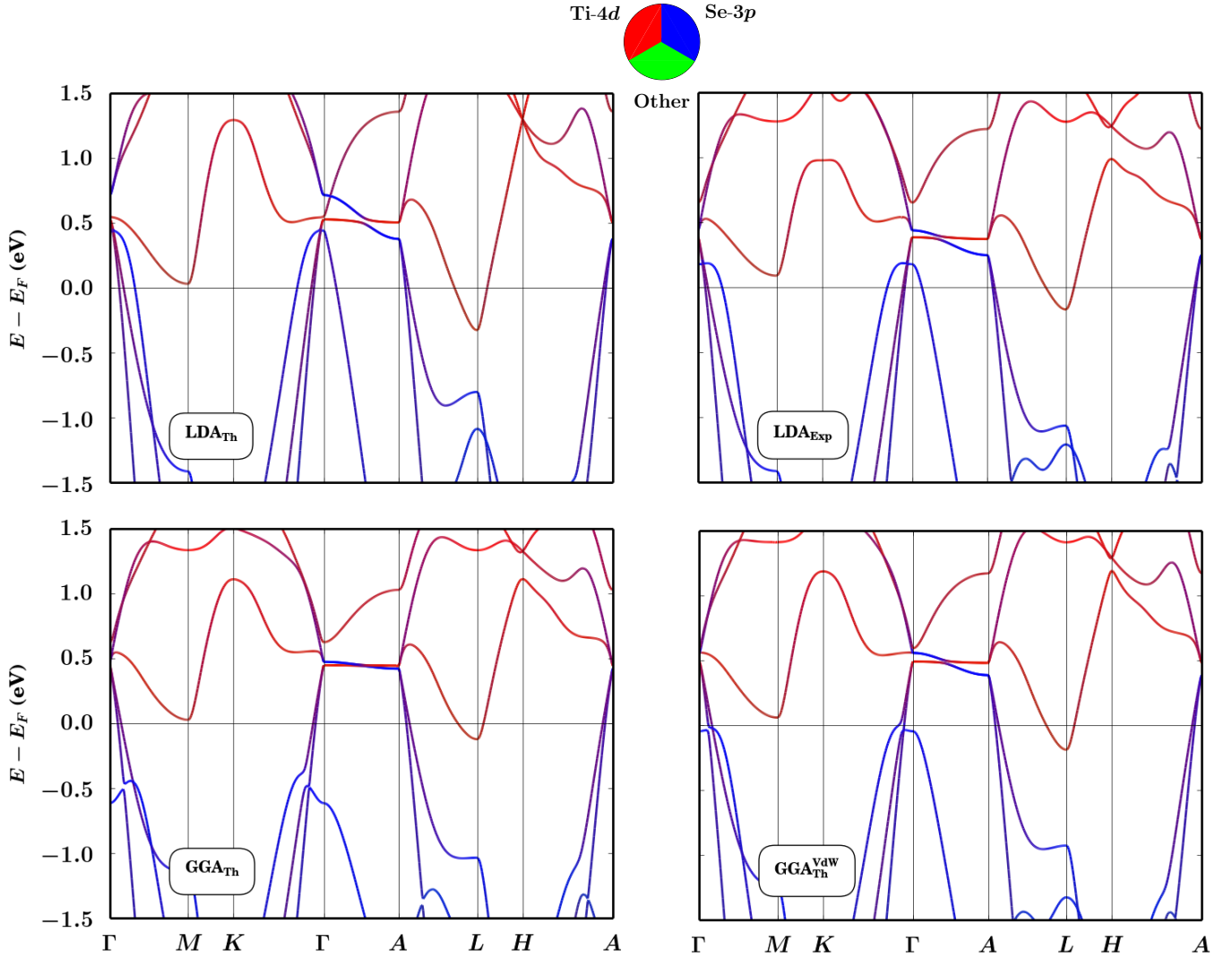


FIG. 8. (color online) Band structure of TiSe_2 (undistorted phase) for several cases along a BZ high-symmetry line (*cf.* Fig. 2). The atomic/orbital character of bands is expressed by using different colors. Starting from the upper left-hand figure, the dimension of the cell along c increases clockwise. Only in the LDA_{Th} case the system does not have an instability.

\mathbf{K} in the SBZ, which is one-eighth of the original BZ. Nevertheless, the function $\Psi_{\mathbf{K},J}$ is made of eight contributions $\psi_{\mathbf{k}_i}^{\mathbf{K},J}$ which are functions pseudo-periodic on the original lattice and whose pseudo-momenta \mathbf{k}_i are obtained by unfolding \mathbf{K} to the original BZ:

$$\Psi_{\mathbf{K},J} = \sum_{i=1}^8 \psi_{\mathbf{k}_i}^{\mathbf{K},J} \quad (15)$$

The spectral weights $\omega_{\mathbf{k}_i}^{\mathbf{K},J}$:

$$\omega_{\mathbf{k}_i}^{\mathbf{K},J} \equiv \|\psi_{\mathbf{k}_i}^{\mathbf{K},J}\|^2 \quad \sum_{i=1}^8 \omega_{\mathbf{k}_i}^{\mathbf{K},J} = 1 \quad (16)$$

can be used to evaluate the contributions to $\Psi_{\mathbf{K},J}$ coming from different points of the original BZ (see appendix A).

From geometrical considerations we see that in our case the SBZ can be unfolded into eight regions of the BZ centered around the points Γ, A, L_i, M_i , respectively, and we can use this property to label the corresponding unfolding weights. Moreover, due to the threefold symmetry of the system, for a point \mathbf{K} it is convenient to sum the contributions coming from the three equivalent L_i points, and the same for the contributions coming from the three M_i points: in this way we have four contributions of type Γ, L, M, A depending on the BZ portion they came from. In Fig. 11 the weights of these four contributions on the bands are shown by means of a color code. In this way we easily recognize, for example, that the characteristic band configuration under E_F in Γ_{sc} has a pure L character.

A complementary method to describe the $2 \times 2 \times 2$ distortion in the frame of the original translation sym-

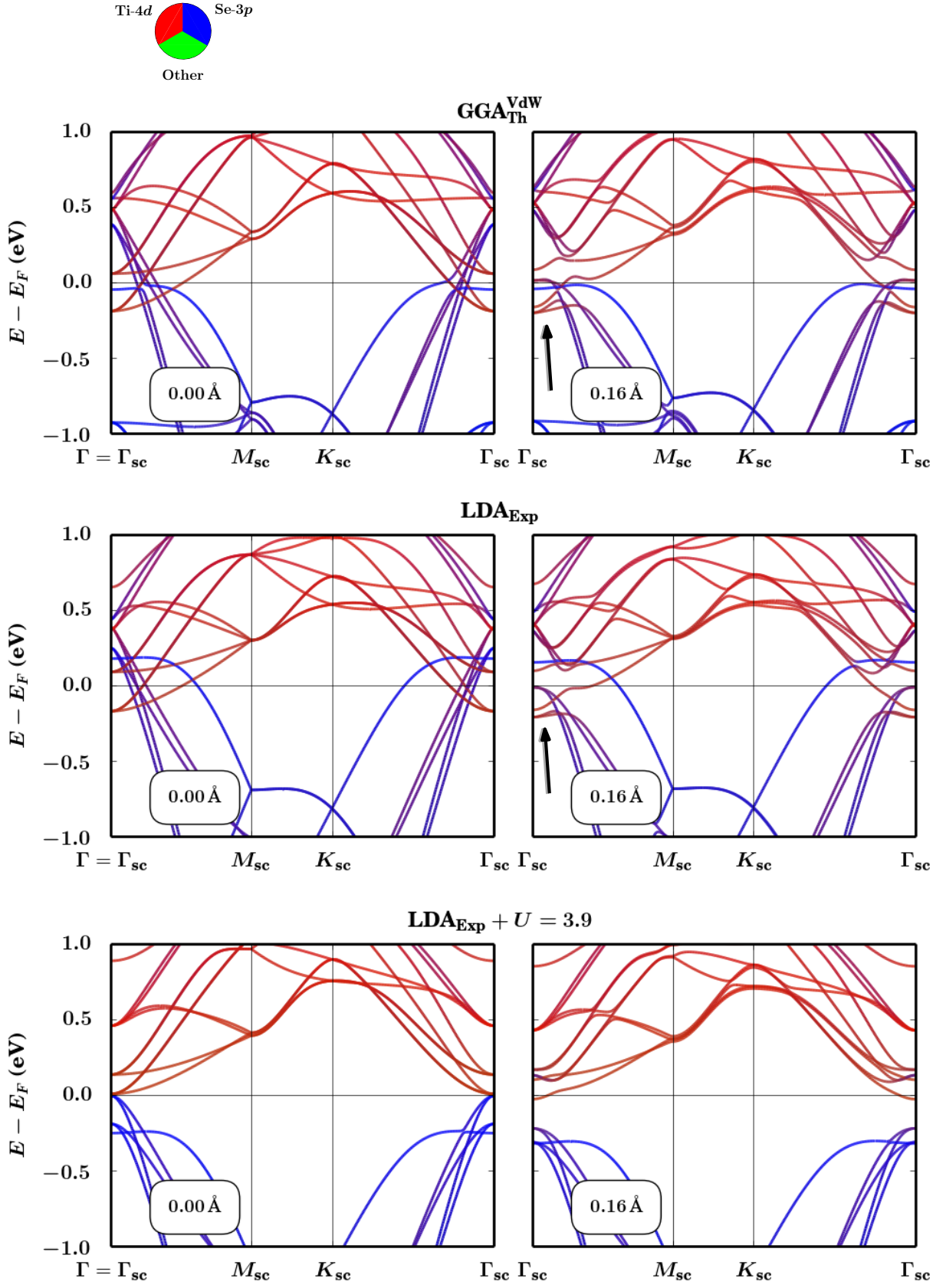


FIG. 9. (color online) DFT bands, with orbital character, of the $2 \times 2 \times 2$ super-lattice along the high symmetry line $\Gamma_{sc} M_{sc} K_{sc} \Gamma_{sc}$ of the super-cell Brillouin zone. Left-hand panels: undistorted configuration ($\|d\| = 0.00 \text{ \AA}$). Right-hand panels: distorted configuration ($\|d\| = 0.16 \text{ \AA}$). An arrow highlights, in two cases, the effect of the repulsion between two Ti-3d bands.

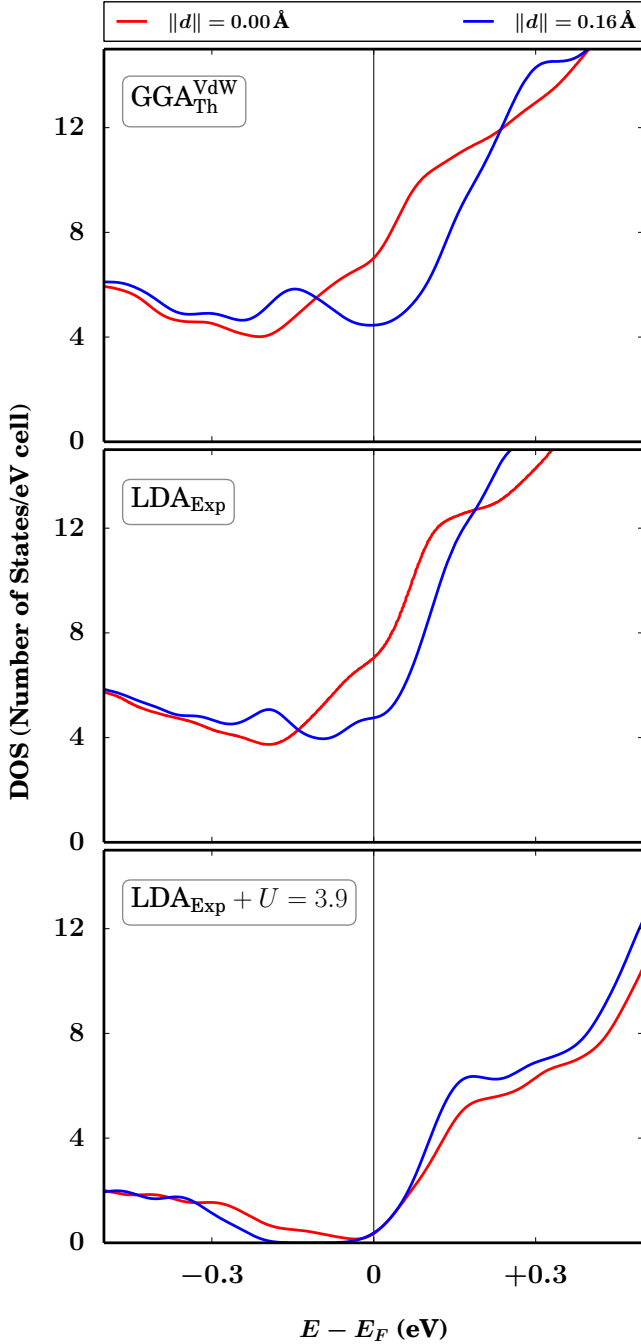


FIG. 10. (color online) Density of states around the Fermi level for three cases in the undistorted (red line) and distorted (green line) phase.

metry (and best suited to make a direct comparison with ARPES experiments) is to unfold the superlattice band structure from SBZ to the original BZ^{32,33}. This consists in plotting for the points \mathbf{k} of a line in the BZ the energy bands $E_{\mathbf{K},J}$ of the distorted system with an intensity $I_{\mathbf{k}}^{K,J}$ equal to the spectral weights $\omega_{\mathbf{k}}^{K,J}$ (for $I_{\mathbf{k}}^{K,J} = 0$ we have full transparency, *i.e.* no band, and for $I_{\mathbf{k}}^{K,J} = 1$

full opacity). In this way the displacement of the atoms is observed as a distortion, smearing and fade of the original bands, plus the appearance of new ghost bands. In Fig. 12 the unfolded bands with the orbital character are shown. In order to ease the comparison with the undistorted phase we also superimpose the unfolded bands on the original band structure. From these figures we can clearly see what is principal effect of the $3L$ distortion: the Ti-4d bands which were crossing the Fermi level now open a gap whereas the Se-3p bands essentially remain unaffected. Moreover we see the appearance of a ghost band in L which gives the characteristic structure we have already discussed.

V. COMPARISON WITH ARPES

A. LDA_{Exp} and $\text{GGA}_{\text{Th}}^{\text{VdW}}$

In the previous sections we analyzed the kind of distortion which lowers the total energy of the system and the consequent changes in the electronic structure as they are found by ab-initio DFT calculations. In this section we compare the results of the calculated band structure and the ARPES data taken from Ref. 34. In Fig. 13 we show the DFT bands for the undistorted and distorted phases superimposed on the ARPES data taken at high ($T = 300$ K) and low ($T = 35$ K) temperature, respectively. Due to the indetermination of \mathbf{k}_z in the ARPES, and the substantial \mathbf{k}_z dispersion in the electronic structure, we consider the DFT bands along the two directions $\Gamma - M$ and $A - L$ in BZ. In the high temperature case we simply plot the bands along these two lines for the undistorted system and in the low temperature case we plot the $2 \times 2 \times 2$ bands of the distorted structure unfolded to BZ along these two directions. In this second case, in order to ease the comparison with the underlying figure, we slightly enhanced the intensity of the unfolded bands by scaling the whole transparency by a factor $f = 4$:

$$I_{\mathbf{k}}^{K,J} = f \cdot \omega_{\mathbf{k}}^{K,J} \quad (17)$$

As we can see, the effect of the distortion on the theoretical bands can be considered in reasonable agreement with the experimental data for the low temperature phase (in particular it is remarkable that the Mexican-hat found in L seems to reproduce an experimentally observed feature). Nevertheless, there are features in the bands which seem to be not compatible with the ARPES findings. This is even more evident for the high temperature phase since in this case the ARPES data are not in good agreement with the bands of the undistorted structure. In the second case, a possible reason for the mismatch could be the effect of phonon quantum fluctuations on the electronic structure, which are obviously stronger when we consider higher temperatures and which are not taken into account in our “zero temperature” calculations. More generally, a possible explanation for the not

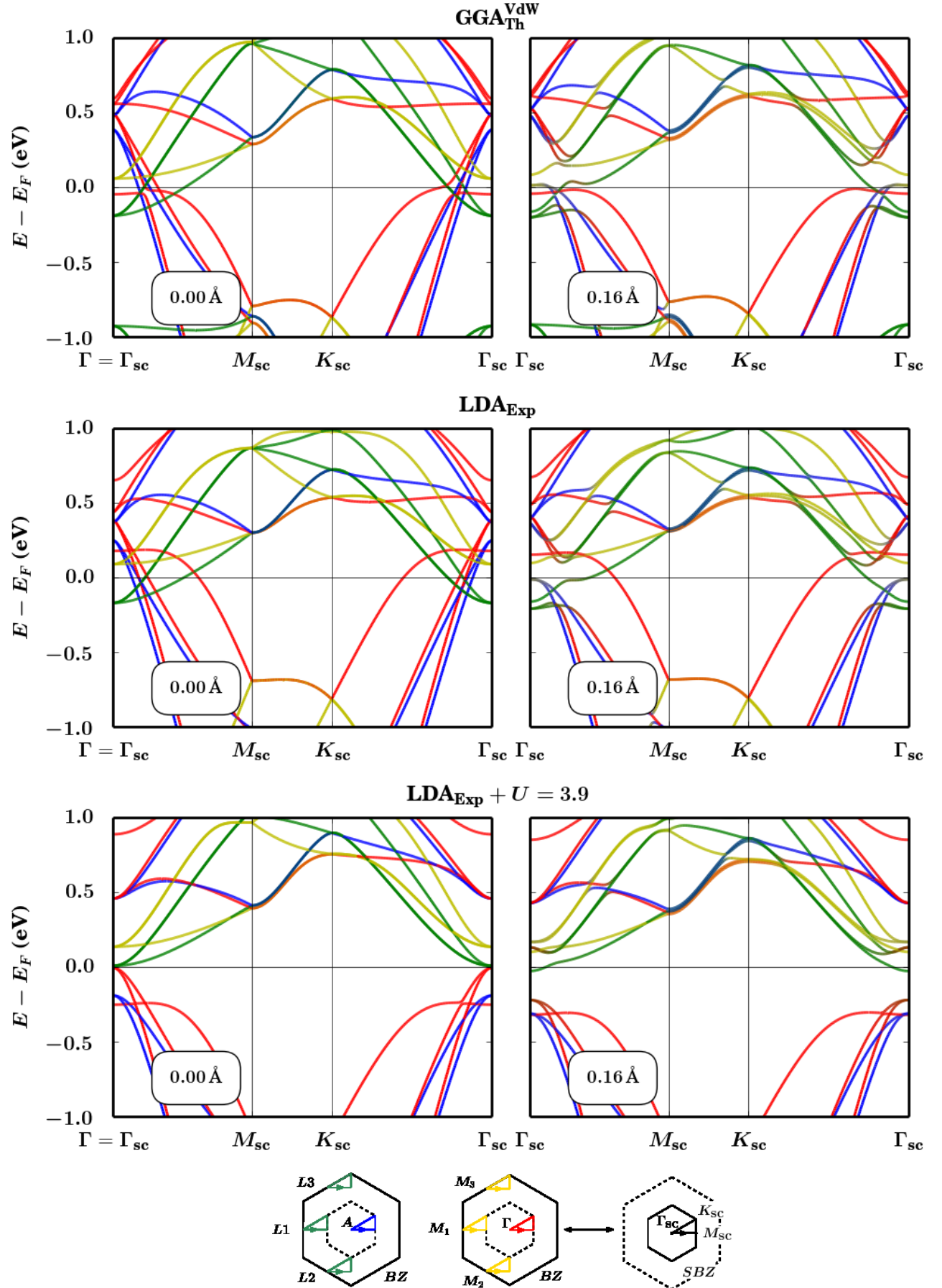


FIG. 11. (color online) DFT bands of the $2 \times 2 \times 2$ super-lattice along the high symmetry line $\Gamma_{sc}M_{sc}K_{sc}\Gamma_{sc}$ of the super-cell Brillouin zone. Left-hand panels: undistorted configuration ($\|d\| = 0.00 \text{ \AA}$). Right-hand panels: distorted configuration ($\|d\| = 0.16 \text{ \AA}$). The colors indicate the weights of the corresponding eigenfunctions on different parts of the $1 \times 1 \times 1$ Brillouin zone.

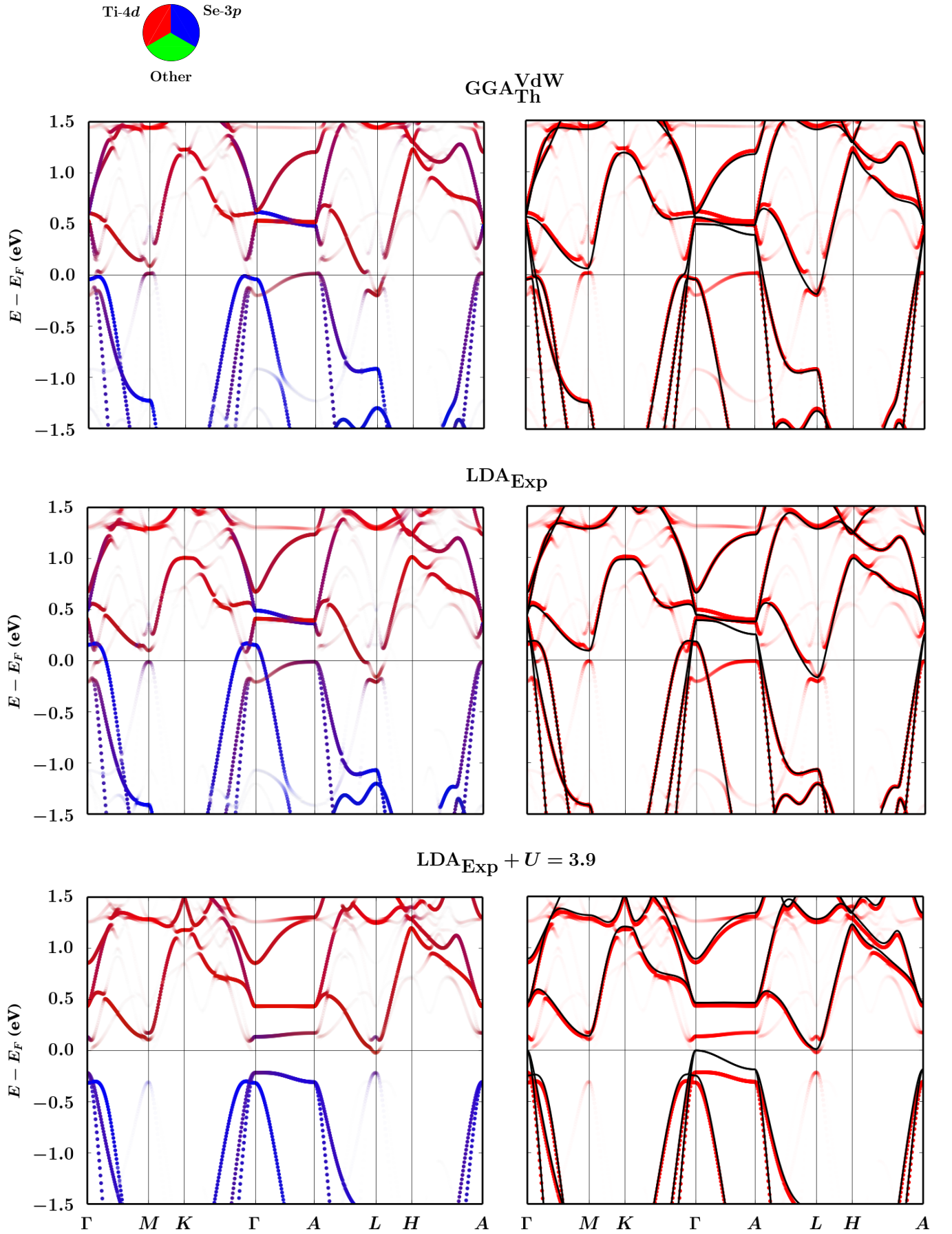


FIG. 12. (color online) Unfolded bands for three cases. Left-hand panels: unfolded bands for the distorted phase on a high symmetry line of the original Brillouin zone with the orbital characters highlighted by colors. Right-hand panels: unfolded bands (in red) superimposed on the undistorted bands (in black) along the same line.

perfect agreement between ARPES and the calculated bands in both the phases could be the effect of the correlation due to the localized d orbitals of Ti (correlation which is not taken into account in a pure DFT calculation). We explored this possibility by using the DFT+ U method (in particular the LDA+ U method) and in the next section we show the results of this analysis.

B. LDA_{Exp}+ U

As explained in Sec. II, we considered the Hubbard-like correction to the electronic structure of LDA_{Exp}. We used the experimental cell, the internal theoretical coordinates obtained with LDA and, on the top of this, the U correction for the Ti- d orbitals. The most evident effect of introducing U is to open a gap between the bands with the result of obtaining, for $U \simeq 3.8$ eV, a metal-insulator transition (see Fig. 14). Motivated by this result, we found appropriate to estimate ab-initio the proper value of U by using a self-consistent procedure. In a few steps we obtained the converged value $U = 3.902$ eV for which the system is in an insulating phase with a small gap of approximately 0.014 eV (see Fig. 14). This result is in line with a recent observation³⁵, although another optical experiment³⁶) has found a semi-metallic state in both the high-temperature and low-temperature phases. Nevertheless, the LDA_{Exp}+ U result seems to be closer to the experimental observations than the large negative gap obtained with pure DFT calculations.

We used the same value of U also for the distorted structure found in the LDA_{Exp} case. We observe that the distortion has, on the electronic bands, the same qualitative effect already observed without U , the shift of the Ti- d bands now increasing the initial small band gap up to a value of approximately 0.2 eV (see Fig. 9, 10, 11, 12). In the lowest panel of Fig. 13 we compare the calculated LDA_{Exp} + U bands with ARPES data: now the theoretical results for both the distorted and undistorted structure are in very good agreement with experimental data taken at high and low temperature, respectively.

According to these results, the correction provided by U seems to solve even the last dubious results regarding the comparison between the DFT electronic structure and the experiment, in particular by giving a perfect match between the theoretical bands and the ARPES data. Unfortunately, a serious drawback of this approach is that the presence of U eliminates the instability.

In Fig 15 we show the lowest phonon frequency ω_L (ω_M) in L (M) as a function of U calculated by using the finite-difference method. When a phonon frequency ω is imaginary we conventionally indicate it with the negative value $-|\omega|$. We considered the LDA system with experimental cell and internal coordinates now obtained by relaxing the atomic positions for each value of U . It can be observed that the frequencies, which are negative (*i.e.* imaginary) for $U = 0$ eV, increase as we increase U and begin to have a positive value around

$U \simeq 2.5$ eV for ω_L and $U \simeq 1.5$ eV for ω_M . A phonons converged calculation with this method was revealed to be extremely costly, especially for values of U close to the metal-insulator transition, so we also explicitly verified that the total energy of the system increases as we move the atoms along the expected distortion pattern. We performed similar tests also for the other cases and we reached a similar conclusion: the DFT+ U system is not unstable anymore for the value of U which seems to return the best agreement between the undistorted bands and the high temperature ARPES data (notice that this value is functional-dependent, U being not a physical measurable quantity).

At this point an intriguing question arises: on one hand it seems that we are able to correct the energy band structure by using U , but on the other hand the same correction spoils the prediction of the instability driven by the electron-phonon coupling, a prediction whose reliability, in turn, strongly depends on the correctness of the energy evaluation.

A first possible explanation for this apparent paradox could be in the simplistic approach used to describe the structural instability with U . In general, the energy of a DFT+ U system (with cell fixed) is given by a function $\mathcal{E}(\mathbf{R}_i, U_j)$ of the atomic positions \mathbf{R}_i and the values U_j for the orbitals. Moreover, for a certain atomic configuration \mathbf{R}_i we have a proper value $U_j = \mathcal{U}_j(\mathbf{R}_i)$ for the Hubbard terms. So the total energy of the system as a function of the atomic positions, $E(\mathbf{R}_i)$, is given by:

$$E(\mathbf{R}_i) = \mathcal{E}(\mathbf{R}_i, \mathcal{U}_j(\mathbf{R}_i)) \quad (18)$$

and when we consider the forces and the force constant matrix (through the first and second derivative of E with respect to the positions \mathbf{R}_i , respectively) we should take into account the full dependency on the atomic positions. On the contrary, a commonly accepted procedure is to neglect the dependence of the Hubbard terms on \mathbf{R}_i and to move the atoms by keeping fixed the values of U_j found for the undistorted system. This is the approach we considered in our study but its correctness seems to be questionable in this case since even a small variation of U (so small that it does not affect the energy bands position) leads to a total energy variation which is huge if compared with the energy decrease obtained with the distortion. For example, during the self-consistent calculation of U , we found that for $\Delta U \simeq 1$ meV the system has a variation of the total energy $\Delta E \simeq 8$ meV.

Therefore, in general, we expect that in order to make a proper structural analysis of TiSe₂ in the DFT+ U scheme it is necessary to take into account the full position dependence (and consider that in the distorted phase we have two not equivalent Ti sites with, in principle, two different values of U). But it also means that, for example, a careful study of the convergence of U with the size of the supercell used to perform the perturbative calculation should be done. Nonetheless, it seems that, in general, the precision required for the value of U (at least 10^{-5} eV) is unrealistic and probably rules out the

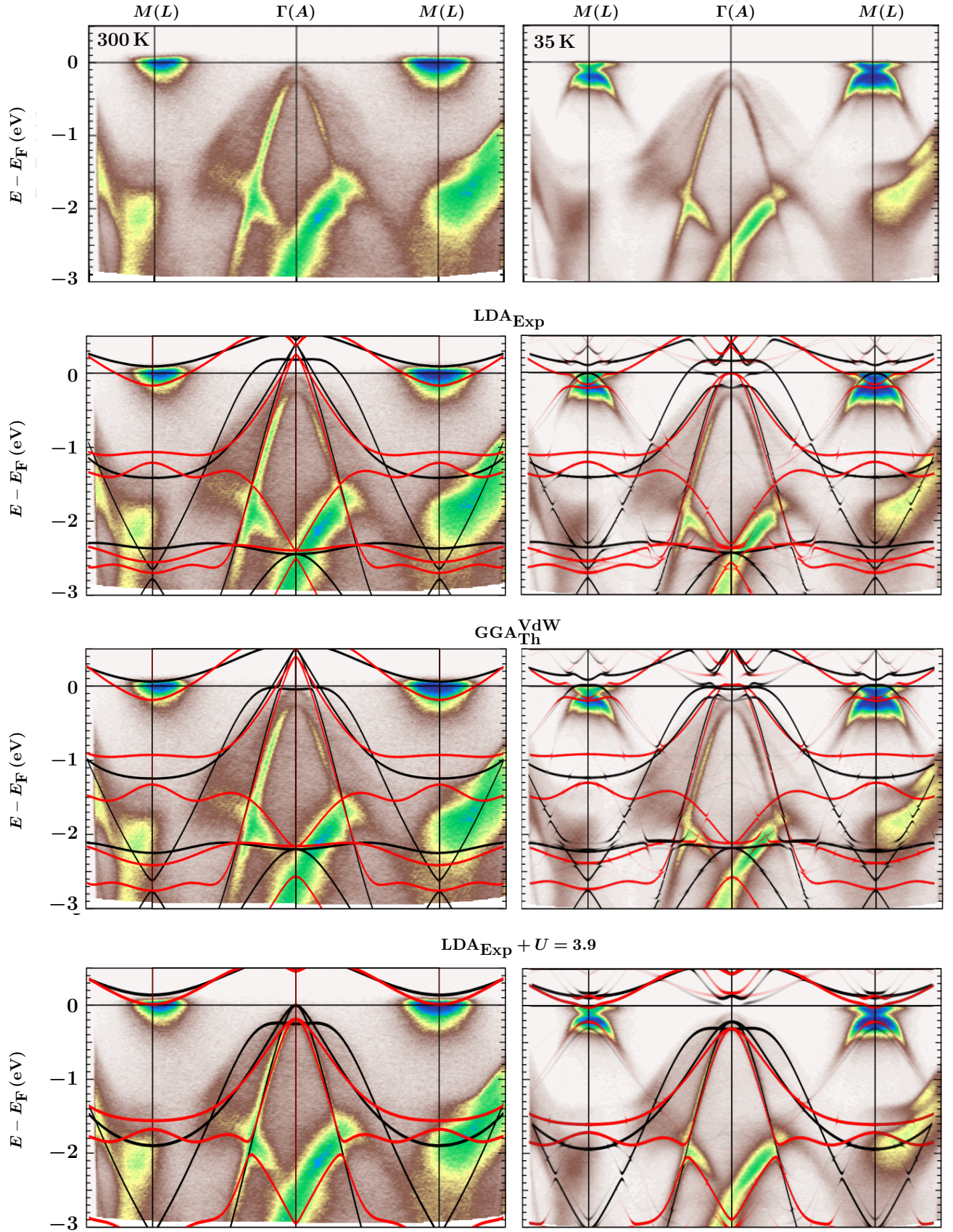


FIG. 13. (color online) Comparison with ARPES data (from Ref. 34) in three cases. First row: ARPES data taken at high temperature (left-hand panel, $T = 300$ K) and low temperature (right-hand panel, $T = 35$ K). Last three rows: DFT bands superimposed on the ARPES data. Black lines: $\Gamma - M$ direction in BZ. Red lines: $A - L$ direction in BZ. In the high temperature cases the bands of the undistorted structure are plotted. In the low temperature cases the $2 \times 2 \times 2$ bands of the distorted structure unfolded to the original BZ are plotted. The intensity of the unfolded ghost bands have been slightly enhanced in order to ease the comparison with the ARPES figure (see main text).

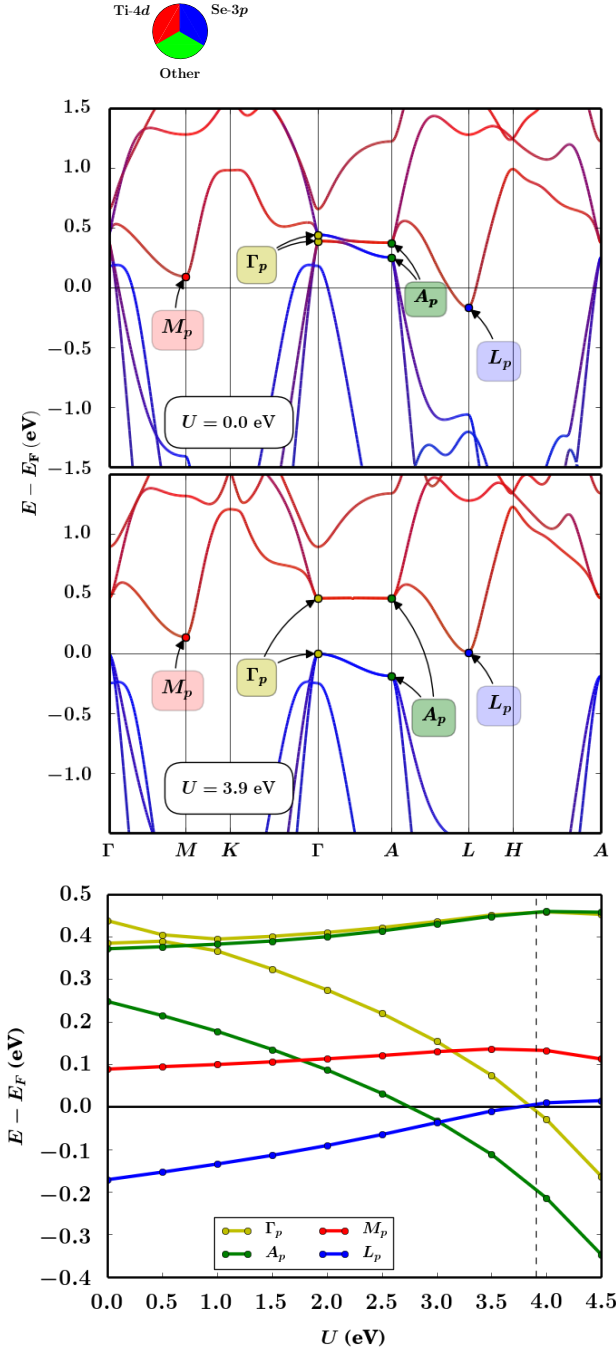


FIG. 14. (color online) Effect of U on the bands. In the last figure the vertical dashed line indicates the final self-consistent value $U \simeq 3.9$ eV, which corresponds to an insulating phase with a small gap of approximatively 0.014 eV.

use of a DFT+ U method in this form.

A second consideration relies on the variation shown by the frequencies $\omega_L(U)$ and $\omega_M(U)$ with U . In fact, we observe a monotonic increase of these two quantities until the points A_p and Γ_p in Fig. 14 go below the point L_p and the point M_p , respectively; after that the value of the frequencies essentially remain constant. So it seems

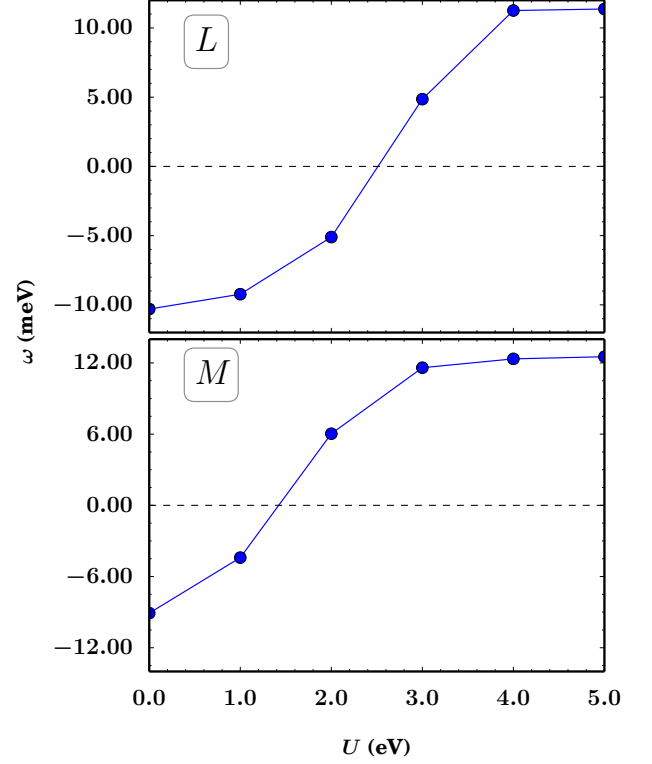


FIG. 15. (color online) Lowest phonon frequency in L and M as a function of U , for the LDA+ U system with experimental cell and theoretical internal coordinates.

that U removes the instability because of the change in the relative positions of the bands. Thus, it could be impossible to maintain the lattice instability and, at the same time, reproduce the high temperature ARPES experiment. This would confirm the difficulty of predicting the high temperature energy dispersion with a DFT(+ U) band calculation.

VI. CONCLUSIONS

In this work we have presented a first-principle study of the charge-density wave in TiSe_2 by using first-principle DFT calculations. We have considered several local functionals and both experimental and theoretical cell parameters.

We have shown that the results are robust with respect to the local functional used, whereas they depend essentially on the distance between the layers, a larger distance corresponding to an higher instability. In fact, no instability is observed in the LDA case with zero theoretical pressure, in this case the distance between the layers being smaller than the experimental one. On the contrary, as long as the cell parameters are in agreement with the experiments, or even larger, the calculations reproduce not only the structural instability but also the triple- \mathbf{q}_L distortion observed in neutron diffraction ex-

periments. We have also explicitly analyzed the role of the interaction between layers by considering distortions of type M and L . We have concluded that, in both the points of the BZ, is the triple- \mathbf{q} distortion which always gives the most energetically favorable configuration, elucidating the importance of the in-plane displacements in order to lower the total energy. Nevertheless, as long as the layers are close enough to have a significant interaction, the L distortions are always more favorable than the M ones, meaning that the intra-layer interaction plays a not negligible role in the CDW transition.

We have also analyzed the changes in the electronic structure of the system with the CDW formation. In the experiment, the phase transition is accompanied by changes in the transport properties. We have found modifications in the calculated bands near the Fermi level, with a resulting depletion in the DOS, which are compatible with the changes measured in the resistivity. The bands for the superstructure have also been unfolded into the undistorted BZ in order to analyze their evolution with the phase transition and compare them with the findings of an ARPES experiment. We have shown that the unfolded bands of the distorted structure are in reasonable agreement with the low-temperature ARPES data. Nevertheless, the bands for the undistorted phase are in not good agreement with ARPES.

In order to correct the mismatch between ARPES data and band calculations we have explored the role of the correlation of the Ti- d electrons by performing an LDA+ U calculation. We have estimated ab-initio, self-consistently, the value of the parameter U for the localized Ti- d orbital in the LDA_{Exp} undistorted structure. For this value of U , the Hubbard-like correction opens a small indirect gap in the electronic bands of the undistorted phase, whereas a pure DFT calculations provides a semi-metallic configuration with a large negative gap. This result is compatible with some recent experiments. More importantly, the LDA+ U bands are in very good agreement with the results of an high-temperature ARPES experiment. By using the same value of U for the distorted structure, we have shown that the CDW increases the size of the band gap. The unfolded bands of the distorted phase are also in good agreement with the low-temperature ARPES data.

The drawback of the LDA+ U approach is that the U correction removes the instability, the phonon frequency in M and L becoming real as we increase the value of U . A possible explanation for this effect has been identified in the neglected, but in principle existing, dependence of the value of U from the atomic positions. On the other hand, the loss of the instability could be the correct result of the electronic bands displacement caused by the local-chemistry correction given by U in TiSe₂. This would be compatible with the suppression of the CDW observed in the ternary crystals TiS _{x} Se_{2- x} for $x > 0.95$ ¹. In fact, at variance with TiSe₂, TiS₂ has no CDW instability, but the electronic structures of these two systems are very similar, the relative position of the valence and conduc-

tion band being the main relevant difference: while TiSe₂ is a small-gap semiconductor/semi-metal, TiS₂ is a semiconductor with a bigger gap.

In conclusion, we have shown that the CDW phase in TiSe₂ can be fully predicted by considering only the electron-phonon coupling and neglecting any electron many-body effect. An incongruence remains between the DFT bands and the experiments, especially for the high-temperature phase. The simple correction provided by the Hubbard-like U term corrects this aspect, but it does not provide a fully coherent picture as it spoils the phonon instability. This represents an open issue which deserves to be examined in future studies.

ACKNOWLEDGMENTS

The authors acknowledge financial support of the Graphene Flagship and of the French National ANR funds within the *Investissements d'Avenir* program under reference ANR-13-IS10-0003-01. Computer facilities were provided by PRACE, CINES, CCRT, IDRIS and by the project Equip@Meso (reference ANR-10-EQPX-29-01). The authors are grateful to K. Rossnagel, for having supplied to them the image data of ARPES experiment as well as detailed explanations of the measures realized, and to M. Cococcioni for useful discussions about the DFT+ U method. R. Bianco thanks L. Paulatto for the support given in the use of QUANTUM ESPRESSO package.

Appendix A: Folding and Unfolding, definition of the spectral weights

We label with \mathcal{R} and $\tilde{\mathcal{R}}$ the direct and reciprocal lattice vectors of the unit cell, respectively. Moreover, we define \mathcal{R}_{sc} and $\tilde{\mathcal{R}}_{sc}$ as the direct and reciprocal lattice vectors of the $2 \times 2 \times 2$ supercell, respectively. We find eight vectors $\mathbf{G}_i \in \tilde{\mathcal{R}}_{sc}$ (defined up to a vector of $\tilde{\mathcal{R}}$) whose differences are not vectors of $\tilde{\mathcal{R}}$:

$$\begin{aligned} \mathbf{G}_i &\in \tilde{\mathcal{R}}_{sc} \\ \mathbf{G}_i - \mathbf{G}_j &\notin \tilde{\mathcal{R}} \end{aligned} \quad (\text{A1})$$

In the coordinates relative to $\tilde{\mathcal{R}}$ it is, for example:

$$\begin{aligned} \mathbf{G}_0 &= (0.0, 0.0, 0.0) & \mathbf{G}_1 &= (0.0, 0.0, 0.5) \\ \mathbf{G}_2 &= (0.5, 0.0, 0.0) & \mathbf{G}_3 &= (0.5, 0.0, 0.5) \\ \mathbf{G}_4 &= (0.0, 0.5, 0.0) & \mathbf{G}_5 &= (0.0, 0.5, 0.5) \\ \mathbf{G}_6 &= (0.5, 0.5, 0.0) & \mathbf{G}_7 &= (0.5, 0.5, 0.5) \end{aligned} \quad (\text{A2})$$

By using these vectors we can unfold a general $\mathbf{K} \in \text{SBZ}$ to eight $\mathbf{k}_i \in \text{BZ}$:

$$\mathbf{k}_i = \mathbf{K} + \mathbf{G}_i \quad (\text{A3})$$

and write:

$$\Psi_{\mathbf{K},J} = \sum_{i=1}^8 \mathcal{P}_{\mathbf{k}_i}(\Psi_{\mathbf{K},J}) \quad (\text{A4})$$

where $\mathcal{P}_{\mathbf{k}_i}$ is the projector on the space of the Bloch functions having pseudo-momentum \mathbf{k}_i with respect to \mathcal{R} , that is $\mathcal{P}_{\mathbf{k}_i}(\Psi_{\mathbf{K},J})$ is a function $\psi_{\mathbf{k}_i}^{\mathbf{K},J}(\mathbf{x})$ such that:

$$\psi_{\mathbf{k}_i}^{\mathbf{K},J}(\mathbf{x} + \mathbf{r}) = e^{i\mathbf{k}_i \cdot \mathbf{r}} \psi_{\mathbf{k}_i}^{\mathbf{K},J}(\mathbf{x}) \quad \forall \mathbf{r} \in \mathcal{R} \quad (\text{A5})$$

The square modulus of $\mathcal{P}_{\mathbf{k}_i}(\Psi_{\mathbf{K},J})$ is, by definition, the unfolded weight $\omega_{\mathbf{k}_i}^{\mathbf{K},J}$ of the superlattice band (\mathbf{K}, J) in \mathbf{k}_i :

$$\omega_{\mathbf{k}_i}^{\mathbf{K},J} \equiv \|\mathcal{P}_{\mathbf{k}_i}(\Psi_{\mathbf{K},J})\|^2 \quad (\text{A6})$$

In order to plot the unfolded energy spectrum along an high-symmetry line of BZ, for each \mathbf{k}_0 of this line we considered the superstructure eigenvectors $\Psi_{\mathbf{K}(\mathbf{k}_0),J}$ and eigenvalues $E_{\mathbf{K}(\mathbf{k}_0),J}$, where $\mathbf{K}(\mathbf{k}_0)$ is the SBZ point where $\mathbf{k}_0 \in \text{BZ}$ fold into:

$$\mathbf{K}(\mathbf{k}_0) = \mathbf{k}_0 - \mathbf{G}_0 = \mathbf{k}_0 \quad (\text{A7})$$

Notice that, properly speaking, \mathbf{k}_0 and $\mathbf{K}(\mathbf{k}_0)$ are not simple vectors: they represent classes of vectors defined up to the sum with an element in $\tilde{\mathcal{R}}$ and $\tilde{\mathcal{R}}_{\text{sc}}$, respectively; so even if the representatives \mathbf{k}_0 and $\mathbf{K}(\mathbf{k}_0)$ are equal they refer to different set of vectors. Then we plotted the bands $E_{\mathbf{K}(\mathbf{k}_0),J}$ with intensity:

$$I_{\mathbf{k}_0}^{\mathbf{K}(\mathbf{k}_0),J} = \omega_{\mathbf{k}_0}^{\mathbf{K}(\mathbf{k}_0),J} \quad (\text{A8})$$

$I_{\mathbf{k}_0}^{\mathbf{K}(\mathbf{k}_0),J} = 0$ corresponding to full transparency (no band) and $I_{\mathbf{k}_0}^{\mathbf{K}(\mathbf{k}_0),J} = 1$ to full opacity.

-
- ¹ F. J. Di Salvo, D. E. Moncton, and J. V. Waszczak, Phys. Rev. B **14**, 4321 (Nov 1976), <http://link.aps.org/doi/10.1103/PhysRevB.14.4321>
 - ² M. Holt, P. Zschack, H. Hong, M. Y. Chou, and T.-C. Chiang, Phys. Rev. Lett. **86**, 3799 (Apr 2001), <http://link.aps.org/doi/10.1103/PhysRevLett.86.3799>
 - ³ K. Motizuki, *Structural Phase Transitions in Layered Transition Metal Compounds*, Physics and Chemistry of Materials with A (Springer, 1986) ISBN 9789027721716, <http://books.google.fr/books?id=jH9u5Qc-m1oC>
 - ⁴ S. Hellmann, T. Rohwer, M. Kallne, K. Hanff, C. Sohr, A. Stange, A. Carr, M. Murnane, H. Kapteyn, L. Kipp, M. Bauer, and K. Rossnagel **3** (2012)
 - ⁵ K. Rossnagel, Journal of Physics: Condensed Matter **23**, 213001 (2011), <http://stacks.iop.org/0953-8984/23/i=21/a=213001>
 - ⁶ H. Cellier, C. Monney, F. Clerc, C. Battaglia, L. Despont, M. G. Garnier, H. Beck, P. Aebi, L. Patthey, H. Berger, and L. Forró, Phys. Rev. Lett. **99**, 146403 (Oct 2007), <http://link.aps.org/doi/10.1103/PhysRevLett.99.146403>
 - ⁷ J. A. Wilson, physica status solidi (b) **86**, 11 (1978), ISSN 1521-3951, <http://dx.doi.org/10.1002/pssb.2220860102>
 - ⁸ J. A. Wilson, Solid State Communications **22**, 551 (1977), ISSN 0038-1098, <http://www.sciencedirect.com/science/article/pii/0038109877901338>
 - ⁹ H. P. Hughes, Journal of Physics C: Solid State Physics **10**, L319 (1977), <http://stacks.iop.org/0022-3719/10/i=11/a=009>
 - ¹⁰ K. Rossnagel, L. Kipp, and M. Skibowski, Phys. Rev. B **65**, 235101 (May 2002), <http://link.aps.org/doi/10.1103/PhysRevB.65.235101>
 - ¹¹ E. Morosan, Zandbergen, B. S. Dennis, J. W. G. Bos, Y. Onose, T. Klimczuk, A. Ramirez, N. P. Ong, and R. J. Cava **2** (2006)
 - ¹² A. F. Kusmartseva, B. Sipos, H. Berger, L. Forró, and E. Tutiš, Phys. Rev. Lett. **103**, 236401 (Nov 2009), <http://link.aps.org/doi/10.1103/PhysRevLett.103.236401>
 - ¹³ M. Calandra and F. Mauri, Phys. Rev. Lett. **112**, 049702 (Jan 2014), <http://link.aps.org/doi/10.1103/PhysRevLett.112.049702>
 - ¹⁴ P. Giannozzi, S. Baroni, N. Bonini, M. Calandra, R. Car, C. Cavazzoni, D. Ceresoli, G. L. Chiarotti, M. Cococcioni, I. Dabo, A. Dal Corso, S. de Gironcoli, S. Fabris, G. Fratesi, R. Gebauer, U. Gerstmann, C. Gougousis, A. Kokalj, M. Lazzeri, L. Martin-Samos, N. Marzari, F. Mauri, R. Mazzarello, S. Paolini, A. Pasquarello, L. Paulatto, C. Sbraccia, S. Scandolo, G. Sclauzero, A. P. Seitsonen, A. Smogunov, P. Umari, and R. M. Wentzcovitch, Journal of Physics: Condensed Matter **21**, 395502 (19pp) (2009), <http://www.quantum-espresso.org>
 - ¹⁵ J. P. Perdew and A. Zunger, Phys. Rev. B **23**, 5048 (May 1981), <http://link.aps.org/doi/10.1103/PhysRevB.23.5048>
 - ¹⁶ J. P. Perdew, K. Burke, and M. Ernzerhof, Phys. Rev. Lett. **77**, 3865 (Oct 1996), <http://link.aps.org/doi/10.1103/PhysRevLett.77.3865>
 - ¹⁷ S. Grimme, Journal of Computational Chemistry **27**, 1787 (2006), ISSN 1096-987X, <http://dx.doi.org/10.1002/jcc.20495>
 - ¹⁸ S. Baroni, S. de Gironcoli, A. Dal Corso, and P. Giannozzi, Rev. Mod. Phys. **73**, 515 (Jul 2001), <http://link.aps.org/doi/10.1103/RevModPhys.73.515>
 - ¹⁹ H. J. Monkhorst and J. D. Pack, Phys. Rev. B **13**, 5188 (Jun 1976), <http://link.aps.org/doi/10.1103/PhysRevB.13.5188>
 - ²⁰ C. Riekell, Journal of Solid State Chemistry **17**, 389 (1976), ISSN 0022-4596, <http://www.sciencedirect.com/science/article/pii/S0022459676800084>
 - ²¹ M. Cococcioni and S. de Gironcoli, Phys. Rev. B **71**, 035105 (Jan 2005), <http://link.aps.org/doi/10.1103/PhysRevB.71.035105>
 - ²² B. Himmetoglu, A. Floris, S. de Gironcoli, and M. Cococcioni, International Journal of Quantum Chemistry **114**, 14 (2014), ISSN 1097-461X, <http://dx.doi.org/10.1002/>

- qua.24521
- ²³ D. Alf, Computer Physics Communications **180**, 2622 (2009), ISSN 0010-4655, <http://www.sciencedirect.com/science/article/pii/S0010465509001064>
 - ²⁴ H. J. Kulik, M. Cococcioni, D. A. Scherlis, and N. Marzari, Phys. Rev. Lett. **97**, 103001 (Sep 2006), <http://link.aps.org/doi/10.1103/PhysRevLett.97.103001>
 - ²⁵ M. H. Whangbo and E. Canadell, Journal of the American Chemical Society **114**, 9587 (1992), <http://pubs.acs.org/doi/pdf/10.1021/ja00050a044>, <http://pubs.acs.org/doi/abs/10.1021/ja00050a044>
 - ²⁶ R. A. Jishi and H. M. Alyahyaei, Phys. Rev. B **78**, 144516 (Oct 2008), <http://link.aps.org/doi/10.1103/PhysRevB.78.144516>
 - ²⁷ J. Ishioka, Y. H. Liu, K. Shimatake, T. Kurosawa, K. Ichimura, Y. Toda, M. Oda, and S. Tanda, Phys. Rev. Lett. **105**, 176401 (Oct 2010), <http://link.aps.org/doi/10.1103/PhysRevLett.105.176401>
 - ²⁸ J.-P. Castellán, S. Rosenkranz, R. Osborn, Q. Li, K. E. Gray, X. Luo, U. Welp, G. Karapetrov, J. P. C. Ruff, and J. van Wezel, Phys. Rev. Lett. **110**, 196404 (May 2013), <http://link.aps.org/doi/10.1103/PhysRevLett.110.196404>
 - ²⁹ J. van Wezel, EPL (Europhysics Letters) **96**, 67011 (2011), <http://stacks.iop.org/0295-5075/96/i=6/a=67011>
 - ³⁰ A. Zunger and A. J. Freeman, Phys. Rev. B **17**, 1839 (Feb 1978), <http://link.aps.org/doi/10.1103/PhysRevB.17.1839>
 - ³¹ N. Suzuki, A. Yamamoto, and K. Motizuki, Journal of the Physical Society of Japan **54**, 4668 (1985), <http://dx.doi.org/10.1143/JPSJ.54.4668>, <http://dx.doi.org/10.1143/JPSJ.54.4668>
 - ³² V. Popescu and A. Zunger, Phys. Rev. Lett. **104**, 236403 (Jun 2010), <http://link.aps.org/doi/10.1103/PhysRevLett.104.236403>
 - ³³ W. Ku, T. Berlijn, and C.-C. Lee, Phys. Rev. Lett. **104**, 216401 (May 2010), <http://link.aps.org/doi/10.1103/PhysRevLett.104.216401>
 - ³⁴ T. Rohwer, S. Hellmann, M. Wiesenmayer, C. Sohrt, A. Stange, B. Slomski, A. Carr, Y. Liu, L. M. Avila, M. Kallne, S. Mathias, L. Kipp, K. Rossnagel, and M. Bauer, Nature **471**, 490 (Sep 2011))
 - ³⁵ J. C. E. Rasch, T. Stemmler, B. Müller, L. Dudy, and R. Manzke, Phys. Rev. Lett. **101**, 237602 (Dec 2008), <http://link.aps.org/doi/10.1103/PhysRevLett.101.237602>
 - ³⁶ G. Li, W. Z. Hu, D. Qian, D. Hsieh, M. Z. Hasan, E. Morosan, R. J. Cava, and N. L. Wang, Phys. Rev. Lett. **99**, 027404 (Jul 2007), <http://link.aps.org/doi/10.1103/PhysRevLett.99.027404>

Supplementary material:
Electronic and vibrational properties of TiSe₂ in the
charge-density wave phase from first principles

GEOMETRICAL PARAMETERS IN THE CHARGE-DENSITY WAVE PHASE

In this Supplementary Material we report the geometrical parameters for the distorted phase obtained in the studied cases. The crystal axes a, c of the hexagonal $2 \times 2 \times 2$ supercell are in cartesian coordinates (Angstrom units). The atomic positions α_i are given in crystal coordinates. For each case, we report both the set of parameters obtained first by minimizing the energy along the distortion path (a, c, α^i) and then relaxing the structure $(a_{\text{rlx}}, c_{\text{rlx}}, \alpha_{\text{rlx}}^i)$.

TABLE I. Hexagonal $2 \times 2 \times 2$ supercell parameters in cartesian coordinates for the minimum of the energy along the distortion path (a, c) and subsequent relaxed structure $(a_{\text{rlx}}, c_{\text{rlx}})$.

	a (Å)	c (Å)	a_{rlx} (Å)	c_{rlx} (Å)
LDA _{Exp}	7.080	12.014	7.080	12.014
GGA _{Exp}	7.080	12.014	7.080	12.014
GGA _{Exp} ^{VdW}	7.080	12.014	7.080	12.014
GGA _{Th}	7.072	13.438	7.076	13.456
GGA _{Th} ^{VdW}	7.019	12.331	7.023	12.339

TABLE II. LDA_{Exp} atomic positions corresponding to the minimum along the distortion path (α^i) and subsequent relaxed structure (α_{rlx}^i) . The atomic positions are in crystal coordinates.

	α^1	α^2	α^3	α_{rlx}^1	α_{rlx}^2	α_{rlx}^3
Ti	-0.0000000	-0.0085192	0.0000000	-0.0000000	-0.0085705	0.0000000
Se	0.1695741	0.3362407	0.1247672	0.1694345	0.3362317	0.1249038
Se	0.3333333	0.1666666	-0.1247672	0.3333333	0.1666666	-0.1247564
Ti	0.0000000	0.0085192	0.5000000	0.0000000	0.0085705	0.5000000
Se	0.1637590	0.3304256	0.6247672	0.1637681	0.3305653	0.6249038
Se	0.3333333	0.1666666	0.3752328	0.3333333	0.1666666	0.3752436
Ti	-0.0000001	0.4999998	0.0000000	-0.0000001	0.4999998	0.0000000
Se	0.1637592	0.8333335	0.1247672	0.1637683	0.8332029	0.1249038
Se	0.3333335	0.6637594	-0.1247672	0.3332028	0.6637684	-0.1249038
Ti	-0.0000001	0.4999998	0.5000000	-0.0000001	0.4999998	0.5000000
Se	0.1695743	0.8333335	0.6247672	0.1694347	0.8332029	0.6249038
Se	0.3333335	0.6695745	0.3752328	0.3332028	0.6694348	0.3750962
Ti	0.5085192	0.0085192	0.0000000	0.5085703	0.0085704	-0.0000000
Se	0.6666666	0.3304256	0.1247672	0.6667972	0.3305653	0.1249038
Se	0.8304258	0.1666666	-0.1247672	0.8305654	0.1667973	-0.1249038
Ti	0.4914808	-0.0085192	0.5000000	0.4914297	-0.0085704	0.5000000
Se	0.6666666	0.3362407	0.6247672	0.6667972	0.3362317	0.6249038
Se	0.8362408	0.1666666	0.3752328	0.8362318	0.1667973	0.3750962
Ti	0.4914806	0.4999998	0.0000000	0.4914296	0.4999998	0.0000000
Se	0.6666668	0.8333335	0.1247672	0.6666667	0.8333335	0.1247564
Se	0.8362410	0.6695745	-0.1247672	0.8362320	0.6694348	-0.1249038
Ti	0.5085191	0.4999998	0.5000000	0.5085702	0.4999997	0.5000000
Se	0.6666668	0.8333335	0.6247672	0.6666667	0.8333335	0.6247564
Se	0.8304259	0.6637594	0.3752328	0.8305656	0.6637684	0.3750962

TABLE III. GGA_{Exp} atomic positions corresponding to the minimum along the distortion path (α^i) and subsequent relaxed structure (α_{rlx}^i). The atomic positions are in crystal coordinates.

	α^1	α^2	α^3	α_{rlx}^1	α_{rlx}^2	α_{rlx}^3
Ti	-0.0077212	-0.0077212	0.0000000	-0.0077862	-0.0077862	0.0000000
Se	0.1666666	0.3363905	0.1276883	0.1667914	0.3363670	0.1278971
Se	0.3363906	0.1666666	-0.1276883	0.3363671	0.1667914	-0.1278971
Ti	0.0077212	0.0077212	0.5000000	0.0077862	0.0077862	0.5000000
Se	0.1666666	0.3302759	0.6276883	0.1667914	0.3304242	0.6278971
Se	0.3302760	0.1666666	0.3723117	0.3304244	0.1667914	0.3721029
Ti	0.0077211	0.4999998	0.0000000	0.0077861	0.4999998	0.0000000
Se	0.1666668	0.8333335	0.1276883	0.1666668	0.8333335	0.1277357
Se	0.3302762	0.6636096	-0.1276883	0.3304245	0.6636332	-0.1278971
Ti	-0.0077213	0.4999998	0.5000000	-0.0077863	0.4999998	0.5000000
Se	0.1666668	0.8333335	0.6276883	0.1666668	0.8333335	0.6277357
Se	0.3363908	0.6697242	0.3723117	0.3363672	0.6695759	0.3721029
Ti	0.5000000	0.0077212	0.0000000	0.5000000	0.0077862	-0.0000000
Se	0.6636093	0.3302759	0.1276883	0.6636328	0.3304242	0.1278971
Se	0.8333333	0.1666666	-0.1276883	0.8333333	0.1666666	-0.1277357
Ti	0.5000000	-0.0077212	0.5000000	0.5000000	-0.0077862	0.5000000
Se	0.6697239	0.3363905	0.6276883	0.6695756	0.3363670	0.6278971
Se	0.8333333	0.1666666	0.3723117	0.8333333	0.1666666	0.3722643
Ti	0.4999999	0.4999998	0.0000000	0.4999999	0.4999998	0.0000000
Se	0.6697240	0.8333335	0.1276883	0.6695757	0.8332087	0.1278971
Se	0.8333335	0.6697242	-0.1276883	0.8332086	0.6695759	-0.1278971
Ti	0.4999999	0.4999998	0.5000000	0.4999999	0.4999998	0.5000000
Se	0.6636095	0.8333335	0.6276883	0.6636329	0.8332087	0.6278971
Se	0.8333335	0.6636096	0.3723117	0.8332087	0.6636331	0.3721029

TABLE IV. GGA_{Exp}^{VdW} atomic positions corresponding to the minimum along the distortion path (α^i) and subsequent relaxed structure (α_{rlx}^i). The atomic positions are in crystal coordinates.

	α^1	α^2	α^3	α_{rlx}^1	α_{rlx}^2	α_{rlx}^3
Ti	-0.0074786	-0.0074786	0.0000000	-0.0075626	-0.0075626	0.0000000
Se	0.1666666	0.3362550	0.1275200	0.1667657	0.3362053	0.1276938
Se	0.3362551	0.1666666	-0.1275200	0.3362055	0.1667657	-0.1276938
Ti	0.0074786	0.0074786	0.5000000	0.0075626	0.0075626	0.5000000
Se	0.1666666	0.3304114	0.6275200	0.1667657	0.3305602	0.6276938
Se	0.3304115	0.1666666	0.3724800	0.3305604	0.1667657	0.3723062
Ti	0.0074785	0.4999998	0.0000000	0.0075625	0.4999998	0.0000000
Se	0.1666668	0.8333335	0.1275200	0.1666668	0.8333335	0.1275652
Se	0.3304116	0.6637451	-0.1275200	0.3305605	0.6637948	-0.1276937
Ti	-0.0074787	0.4999998	0.5000000	-0.0075627	0.4999998	0.5000000
Se	0.1666668	0.8333335	0.6275200	0.1666668	0.8333335	0.6275652
Se	0.3362553	0.6695888	0.3724800	0.3362056	0.6694399	0.3723063
Ti	0.5000000	0.0074786	0.0000000	0.5000000	0.0075626	-0.0000000
Se	0.6637448	0.3304114	0.1275200	0.6637945	0.3305602	0.1276937
Se	0.8333333	0.1666666	-0.1275200	0.8333333	0.1666666	-0.1275652
Ti	0.5000000	-0.0074786	0.5000000	0.5000000	-0.0075626	0.5000000
Se	0.6695884	0.3362550	0.6275200	0.6694396	0.3362053	0.6276937
Se	0.8333333	0.1666666	0.3724800	0.8333333	0.1666666	0.3724348
Ti	0.4999999	0.4999998	0.0000000	0.4999999	0.4999998	0.0000000
Se	0.6695886	0.8333335	0.1275200	0.6694397	0.8332344	0.1276938
Se	0.8333335	0.6695888	-0.1275200	0.8332343	0.6694399	-0.1276938
Ti	0.4999999	0.4999998	0.5000000	0.4999999	0.4999998	0.5000000
Se	0.6637449	0.8333335	0.6275200	0.6637946	0.8332344	0.6276938
Se	0.8333335	0.6637451	0.3724800	0.8332343	0.6637948	0.3723062

TABLE V. GGA_{Th} atomic positions corresponding to the minimum along the distortion path (α^i) and subsequent relaxed structure (α_{rlx}^i). The atomic positions are in crystal coordinates.

	α^1	α^2	α^3	α_{rlx}^1	α_{rlx}^2	α_{rlx}^3
Ti	-0.0105614	-0.0105614	0.0000000	-0.0113010	-0.0113010	-0.0000000
Se	0.1666666	0.3376787	0.1152080	0.1672981	0.3376220	0.1155628
Se	0.3376788	0.1666666	-0.1152080	0.3376221	0.1672982	-0.1155628
Ti	0.0105614	0.0105614	0.5000001	0.0113010	0.0113010	0.5000001
Se	0.1666666	0.3289877	0.6152078	0.1672982	0.3296759	0.6155626
Se	0.3289877	0.1666666	0.3847921	0.3296759	0.1672982	0.3844373
Ti	0.0105614	0.4999998	0.0000000	0.0113009	0.4999999	-0.0000000
Se	0.1666666	0.8333331	0.1152080	0.1666665	0.8333331	0.1147726
Se	0.3289877	0.6623209	-0.1152080	0.3296759	0.6623776	-0.1155628
Ti	-0.0105615	0.4999998	0.5000001	-0.0113010	0.4999997	0.5000001
Se	0.1666666	0.8333331	0.6152078	0.1666665	0.8333331	0.6147724
Se	0.3376787	0.6710120	0.3847921	0.3376221	0.6703237	0.3844373
Ti	0.4999999	0.0105614	0.0000000	0.5000000	0.0113009	0.0000000
Se	0.6623210	0.3289877	0.1152080	0.6623777	0.3296759	0.1155628
Se	0.8333332	0.1666666	-0.1152080	0.8333333	0.1666665	-0.1147726
Ti	0.4999999	-0.0105614	0.5000001	0.4999998	-0.0113009	0.5000001
Se	0.6710121	0.3376787	0.6152078	0.6703238	0.3376221	0.6155626
Se	0.8333332	0.1666666	0.3847921	0.8333333	0.1666665	0.3852275
Ti	0.4999999	0.4999998	0.0000000	0.4999998	0.4999998	-0.0000000
Se	0.6710120	0.8333331	0.1152080	0.6703239	0.8327015	0.1155628
Se	0.8333331	0.6710120	-0.1152080	0.8327016	0.6703238	-0.1155628
Ti	0.4999999	0.4999998	0.5000001	0.4999999	0.4999999	0.5000001
Se	0.6623210	0.8333331	0.6152078	0.6623777	0.8327015	0.6155626
Se	0.8333332	0.6623209	0.3847921	0.8327016	0.6623776	0.3844373

TABLE VI. GGA_{Th}^{VdW} atomic positions corresponding to the minimum along the distortion path (α^i) and subsequent relaxed structure (α_{rlx}^i). The atomic positions are in crystal coordinates.

	α^1	α^2	α^3	α_{rlx}^1	α_{rlx}^2	α_{rlx}^3
Ti	-0.0080061	-0.0080061	0.0000000	-0.0081278	-0.0081278	0.0000000
Se	0.1666667	0.3365859	0.1259154	0.1668046	0.3365521	0.1260378
Se	0.3365859	0.1666665	-0.1259154	0.3365520	0.1668043	-0.1260378
Ti	0.0080061	0.0080061	0.4999999	0.0081277	0.0081277	0.4999999
Se	0.1666668	0.3300811	0.6259155	0.1668046	0.3302527	0.6260379
Se	0.3300810	0.1666665	0.3740845	0.3302527	0.1668043	0.3739622
Ti	0.0080059	0.5000000	0.0000000	0.0081277	0.5000000	-0.0000000
Se	0.1666665	0.8333335	0.1259154	0.1666666	0.8333334	0.1258447
Se	0.3300808	0.6634140	-0.1259154	0.3302523	0.6634478	-0.1260378
Ti	-0.0080063	0.5000000	0.4999999	-0.0081281	0.4999999	0.4999999
Se	0.1666665	0.8333335	0.6259155	0.1666666	0.8333335	0.6258448
Se	0.3365856	0.6699188	0.3740845	0.3365518	0.6697473	0.3739622
Ti	0.4999999	0.0080061	0.0000000	0.4999999	0.0081280	0.0000000
Se	0.6634142	0.3300811	0.1259154	0.6634480	0.3302526	0.1260378
Se	0.8333333	0.1666665	-0.1259154	0.8333333	0.1666665	-0.1258447
Ti	0.4999999	-0.0080061	0.4999999	0.4999998	-0.0081279	0.4999999
Se	0.6699191	0.3365859	0.6259155	0.6697475	0.3365521	0.6260379
Se	0.8333333	0.1666665	0.3740845	0.8333333	0.1666666	0.3741553
Ti	0.5000002	0.5000000	0.0000000	0.5000002	0.5000000	0.0000000
Se	0.6699194	0.8333335	0.1259154	0.6697477	0.8331956	0.1260378
Se	0.8333331	0.6699188	-0.1259154	0.8331952	0.6697472	-0.1260378
Ti	0.5000002	0.5000000	0.4999999	0.5000000	0.4999998	0.4999999
Se	0.6634145	0.8333335	0.6259155	0.6634484	0.8331957	0.6260379
Se	0.8333331	0.6634140	0.3740845	0.8331953	0.6634479	0.3739622